

# Renormalisation of quark propagators from twisted-mass lattice QCD at $N_f=2$

B. Blossier<sup>a</sup>, Ph. Boucaud<sup>a</sup>, M. Brinet<sup>b</sup>, F. De Soto<sup>c</sup>, Z. Liu<sup>d,e</sup>, V. Morenas<sup>f</sup>  
O. Pène<sup>a</sup>, K. Petrov<sup>a</sup>, J. Rodríguez-Quintero<sup>g</sup>



<sup>a</sup> Laboratoire de Physique Théorique<sup>1</sup>,

CNRS et Université Paris-Sud XI, Bâtiment 210, 91405 Orsay Cedex, France

<sup>b</sup> Laboratoire de Physique Subatomique et de Cosmologie, CNRS/IN2P3/UJF,  
53, avenue des Martyrs, 38026 Grenoble, France

<sup>c</sup> Dpto. Sistemas Físicos, Químicos y Naturales, Univ. Pablo de Olavide, 41013 Sevilla, Spain

<sup>d</sup> DAMTP, University of Cambridge, Wilberforce Road, Cambridge CB3 0WA, United Kingdom

<sup>e</sup> Institute of High Energy Physics, Chinese Academy of Science, Beijing 100049, China

<sup>f</sup> Laboratoire de Physique Corpusculaire, Université Blaise Pascal, CNRS/IN2P3  
63177 Aubière Cedex, France

<sup>g</sup> Dpto. Física Aplicada, Fac. Ciencias Experimentales, Univ. de Huelva, 21071 Huelva, Spain

---

<sup>1</sup>Unité Mixte de Recherche 8627 du Centre National de la Recherche Scientifique

## Abstract

We present results concerning the non-perturbative evaluation of the renormalisation constant for the quark field,  $Z_q$ , from lattice simulations with twisted mass quarks and three values of the lattice spacing. We use the RI'-MOM scheme.  $Z_q$  has very large lattice spacing artefacts ; it is considered here as a test bed to elaborate accurate methods which will be used for other renormalisation constants. We recall and develop the non-perturbative correction methods and propose tools to test the quality of the correction. These tests are also applied to the perturbative correction method. We check that the lattice spacing artefacts scale indeed as  $a^2 p^2$ .

We then study the running of  $Z_q$  with particular attention to the non-perturbative effects, presumably dominated by the dimension-two gluon condensate  $\langle A^2 \rangle$  in Landau gauge. We show indeed that this effect is present, and not small. We check its scaling in physical units confirming that it is a continuum effect. It gives a  $\sim 4\%$  contribution at 2 GeV.

Different variants are used in order to test the reliability of our result and estimate the systematic uncertainties.

Finally combining all our results and using the known Wilson coefficient of  $\langle A^2 \rangle$  we find  $g^2(\mu^2)\langle A^2 \rangle_{\mu^2 CM} = 2.01(11) \left( \begin{smallmatrix} +0.61 \\ -0.73 \end{smallmatrix} \right) \text{ GeV}^2$  at  $\mu = 10 \text{ GeV}$ , in fair agreement within uncertainties with the value indepently extracted from the strong coupling constant. We convert the non-perturbative part of  $Z_q$  from RI'-MOM to  $\overline{\text{MS}}$ . Our result for the quark field renormalisation constant in the  $\overline{\text{MS}}$  scheme is  $Z_q^{\overline{\text{MS}}\text{pert}}((2 \text{ GeV})^2, g_{\text{bare}}^2) = 0.750(3)(7) - 0.313(20) (g_{\text{bare}}^2 - 1.5)$  for the perturbative contribution and  $Z_q^{\overline{\text{MS}}\text{non-perturbative}}((2 \text{ GeV})^2, g_{\text{bare}}^2) = 0.781(6)(21) - 0.313(20) (g_{\text{bare}}^2 - 1.5)$  when the non-perturbative contribution is included.

DAMTP-2010-88  
LPT-Orsay 10-81  
UHU-FT/10-39  
LPSC-10122  
PCCF-1007

## Contents

<b>1</b>	<b>Introduction</b>	<b>3</b>
<b>2</b>	<b>Running of <math>Z_q</math></b>	<b>7</b>
2.1	Perturbative running . . . . .	7
2.2	Wilson expansion and non-perturbative running . . . . .	7
2.2.1	$\langle A^2 \rangle$ tree level Wilson coefficients for $Z_q$ . . . . .	7
2.2.2	The Wilson coefficients at $O(\alpha^4)$ . . . . .	8

<b>3</b>	<b>The lattice computations</b>	<b>8</b>
3.1	The lattice action . . . . .	8
3.2	The computation of the quark propagator . . . . .	9
3.3	The method of non-perturbative Hypercubic $H(4)$ correction . . . . .	10
3.3.1	The sliding window fit (SWF) . . . . .	12
3.3.2	The one window fit (OWF) . . . . .	12
3.4	Other lattice artefacts . . . . .	12
<b>4</b>	<b>Lattice results and hypercubic corrections</b>	<b>13</b>
4.1	Perturbative correction . . . . .	13
4.1.1	Prescription with $\tilde{p}_\mu$ . . . . .	14
4.1.2	Prescription with $p_\mu$ . . . . .	15
4.1.3	Lessons about the perturbative method . . . . .	15
4.2	Non perturbative hypercubic correction . . . . .	16
4.2.1	Sliding window fit versus one window fit . . . . .	16
4.2.2	Half-fishbone reduction test . . . . .	16
4.2.3	The slopes in $p^{[4]}$ . . . . .	17
<b>5</b>	<b>Running including <math>\langle A^2 \rangle</math> corrections from OPE</b>	<b>18</b>
5.1	Analysis from the non-perturbative hypercubic corrections . . . . .	21
5.1.1	Comparison of the running from the OWF and the SWF . . . . .	21
5.1.2	Dependence on the fitting range . . . . .	21
5.2	Analysis from the perturbative hypercubic corrections . . . . .	22
5.3	Running of $Z_q^{\text{pert}}$ . . . . .	23
5.4	Merging the three lattice spacings. . . . .	24
5.5	Summarizing . . . . .	25
5.6	Conversion to $\overline{\text{MS}}$ . . . . .	26
5.7	Comparison of different estimates for the gluon condensate . . . . .	27
<b>6</b>	<b>Conclusion</b>	<b>29</b>
<b>A</b>	<b>Appendix: The Wilson coefficients at <math>O(a^4)</math></b>	<b>31</b>

# 1 Introduction

Computing matrix elements in lattice Quantum ChromoDynamics (LQCD) needs often the computation of renormalisation constants. Indeed, even if the lattice computation contains only  $O(a^2)$  lattice artefacts, the bare quantities differ from the continuum ones by  $O(g^2) \simeq O(1/\log(a^2))$  which is unacceptable. Renormalisation restores the  $O(a^2)$  accuracy. It is also known since long that these renormalisation constants need to be computed non-perturbatively, using LQCD techniques.

Several non-perturbative methods have been proposed. Let us here concentrate on those based on the MOM scheme. They start from the computation of Green functions of quarks, gluons and ghosts at large enough momenta in a fixed gauge, usually the Landau gauge. This gives the renormalisation constant  $Z(\mu)$  at many values of the scale  $\mu$ . Assuming that our goal is to deliver the renormalisation constant in the  $\overline{\text{MS}}$  scheme at say 2 GeV (a typical phenomenological scale), one must then use results from perturbative QCD to convert MOM into  $\overline{\text{MS}}$  and run to 2 GeV. The running of  $Z_{\text{MOM}}(\mu)$  is a very powerful testing tool: indeed perturbative QCD is only useful if we are in the perturbative regime, i.e. at large enough momenta. The only way to check whether this is the case is to compare lattice data with the perturbative running. In this framework, it turns out that this is not always the case.

Deviations from perturbative running can be analysed via Wilson operator expansion and the Shifman-Vainshtein-Zakharov (SVZ) sum rules. It turns out that the dominant non-perturbative correction in Landau gauge is due to the non vanishing vacuum expectation value of the only dimension-two operator :  $A^2 \equiv A_\mu^a A^{a\mu}$  [1], and that it is not small [2–8]. It is thus necessary to carefully look for the possibility of such a contribution, which appears in the OPE, as a  $1/p^2$  contribution up to logarithmic corrections. The coefficient of this  $1/p^2$  contribution is equal to the vacuum expectation value  $g^2 \langle A^2 \rangle$  times a Wilson coefficient that has to be computed in perturbation theory, and has been up to three loops for propagators [9]. To argue that a measured  $1/p^2$  contribution is a continuum power correction and not a lattice artefact, we must check that the  $1/p^2$  term in the fit scales with lattice spacing when expressed *in physical units*. To further argue that this is indeed due to  $\langle A^2 \rangle$  we must compare the resulting  $\langle A^2 \rangle$  from different quantities and thus check the universality of the condensates which is on the ground of the SVZ technology. The theory of Wilson operator expansion is then constraining: since there exists only one dimension-two operator, provided that it is renormalized with the same prescription for all these quantities, all the different estimates of  $\langle A^2 \rangle$  should coincide within errors, up to  $1/p^4$  corrections, for a given value of  $N_f$  and of the dynamical masses. Of course, its extraction needs the coefficients of the Wilson expansion which are computable in perturbation. To test this universality of the extracted  $\langle A^2 \rangle$  is one of the goals of our program of analysing many different quark and gluon quantities obtained from lattice gauge configurations produced by the European twisted mass collaboration (ETMC). We have also applied a criterium proposed in [10] to validate the way we use operator expansion. This paper makes one of the first steps in such a program.

It is worthwhile also to mention that several authors have elaborated further on the relation between this gauge-dependent gluon condensate, obtained in the Landau gauge, and possible  $1/p^2$ -terms in gauge invariant quantities, and thus on the phenomenological implications, mainly in connection with confinement scenarios, of such a dimension-two condensate [11].

All this can only be done once the lattice artefacts are eliminated or at least under control. The  $O(a^2)$  artefacts can be quite large since we consider large momenta, while finite volume artefacts are minor. There are two main types of  $O(a^2)$  artefacts:  $O(a^2 p^2)$  artefacts which respect the continuum  $O(4)$  rotation symmetry, and hypercubic artefacts which respect the  $H_4$  hypercubic symmetry group but not  $O(4)$ . The latter are effects of the hypercubic symmetry of the lattice

action. We will identify the  $O(a^2p^2)$  artefacts non-perturbatively by doing a fit of the running  $Z(\mu)$  which will include the perturbative running, the  $\langle A^2 \rangle$  power correction and a term proportional to  $a^2p^2$ . Notice that, while the perturbative and  $\langle A^2 \rangle$  running contributions must approximately scale in physical units, the artefacts must scale in lattice units. This is an additional check we shall perform.

Concerning the elimination of hypercubic artefacts, which is better done before the above mentioned running fit, several methods have been proposed in literature: the democratic selection, the perturbative correction and the non-perturbative “egalitarian” one (“egalitarian” because all the points are used on the same footing in this approach). We will discuss this in some detail later and perform extensive comparisons. In particular we will use a new quality test which consists in watching to what extent the “half-fishbone” structure, which raw lattice results for  $Z_q$  always exhibit and which is a dramatic illustration of hypercubic artefacts, are corrected by every method.

Although all the issues raised here concern all the renormalisation constants as well as the QCD coupling constant, we will concentrate in the following on  $Z_q$ , that renormalises the quark field

$$q_R = Z_q^{1/2} q_B \quad (1.1)$$

where  $q_B$  ( $q_R$ ) is the bare (renormalised) quark field. In the RI'-MOM scheme  $Z_q$  is defined by

$$Z_q(\mu^2 = p^2) = \frac{-i}{12p^2} \text{Tr}[S_{bare}^{-1}(p) \not{p}] \quad (1.2)$$

where  $S_{bare}(p)$  is the bare quark propagator. Our goal is to compute that constant from LQCD with twisted Wilson quarks.

In [4,12] a study <sup>2</sup> of  $Z_q$  was performed from LQCD in the case  $N_f = 0$  using both the overlap and Wilson clover fermions. In [12] the exceptional size of hypercubic artefacts was stressed and a non-perturbative elimination of hypercubic artefacts performed along the same principle as what is used here. In [4] the Wilson coefficient of the  $\langle A^2 \rangle$  was computed up to the leading logarithm approximation and applied to estimate the condensate from the LQCD data. The outcome was that a significant non-perturbative contribution from  $\langle A^2 \rangle$  was needed to account for the results. Notice that we do not expect the  $\langle A^2 \rangle$  to be similar or even close in the cases of  $N_f = 0$  and  $N_f = 2$ .

Summarising the above discussion, we do here concentrate on  $Z_q$  because we consider it as a kind of benchmark for the following reasons:

- It has specially large hypercubic artefacts and is thus a good test bed for a correct treatment of these.
- It has a vanishing anomalous dimension at leading order in the Landau gauge: its perturbative running is thus soft.

---

<sup>2</sup>In [4]  $Z_q$  was denoted  $Z_\psi$

- The Wilson coefficient of the  $\langle A^2 \rangle$  condensate is rather large [4, 9], which is an incentive to look carefully for non-perturbative contributions.

In this paper, in order to test deeply the reliability of our results, we will compare many fits: perturbative/non-perturbative hypercubic correction, one-window/sliding-windows non perturbative hypercubic correction, effect of the total fitting range, fitting separately every  $\beta$  and global fit. As a consequence we will proceed as follows:

- We will recall some general formulae concerning the perturbative and non-perturbative running in the continuum
- describe our lattice setting and our non-perturbative “egalitarian” method to eliminate hypercubic artefacts;
- present the results concerning the *perturbative* correction method for hypercubic artefacts and show the quality checks;
- present the results concerning the *non-perturbative* method to correct for hypercubic artefacts and show the quality checks, propose two types of fits, the sliding windows fit (SWF) and the one-window fit (OWF).
- We will perform the running fit on the output of all the previously mentioned hypercubic corrected data, compare the results for the  $g^2\langle A^2 \rangle$  for all these fits, check the scaling of  $g^2\langle A^2 \rangle$ ;
- check the scaling of the  $\propto a^2p^2$  artefacts;
- check the lattice spacing dependence of  $Z_q^{\text{pert}}$ , the perturbative contribution to  $Z_q$ ,  $\propto g^2$ ;
- study the range of variation of our results for  $g^2\langle A^2 \rangle$  from the egalitarian method with one/sliding window(s), with varying fitting ranges, and the perturbative method with two realisations. We extract from there the systematic uncertainty.
- We will join in one plot the three  $\beta$ 's and perform the fit of the running,
- compare the resulting  $g^2\langle A^2 \rangle$  with the one extracted from the strong coupling constant and with quenched estimates, and tested our procedure according to Martinelli-Sachrajda's criterium [10].
- conclude.

## 2 Running of $Z_q$

### 2.1 Perturbative running

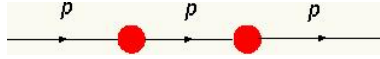
In Landau gauge  $Z_q$  has a vanishing anomalous dimension to leading order, i.e. its running starts at  $O(\alpha^2)$ . The perturbative running has been computed up to four loops [13] and references therein. The needed formulae are accessible on the web site also indicated in ref. [13].

### 2.2 Wilson expansion and non-perturbative running

To handle non-perturbative corrections we use the theory of Operator Product Expansion [14] and its application in estimating power suppressed non-perturbative corrections via vacuum expectation values [15]. In Landau gauge there exists only one dimension-2 operator allowed to have a vacuum expectation value:  $A^2 \equiv \sum_{\mu=1,4}^{a=1,8} A_\mu^a A^{a\mu}$ . The Wilson coefficient of this operator has been computed to leading logarithm in [4] and extensively for all propagators up to  $O(\alpha^4)$  in [9].

#### 2.2.1 $\langle A^2 \rangle$ tree level Wilson coefficients for $Z_q$

In order to give a hint let us just sketch the tree level calculation of that Wilson coefficient.



Consider the above diagram, describing a quark propagating in a constant background gauge field. As a consequence the red bubble represents the interaction of the quark with this background field:  $ig\lambda_a/2 A^a$ . The Feynman rules are then applied as usual. Neglecting the quark mass it gives

$$\begin{aligned} & \frac{-i\not{p}}{p^2} \left( \sum_{\mu=1, a=1}^{\mu=4, a=8} \sum_{\mu'=1, a'=1}^{\mu'=4, a'=8} ig \frac{\lambda_a}{2} A_\mu^a \gamma^\mu \frac{-i\not{p}}{p^2} ig \frac{\lambda_{a'}}{2} A_{\mu'}^{a'} \gamma^{\mu'} \delta_{aa'} \delta_{\mu\mu'} \right) \frac{-i\not{p}}{p^2} \\ & = -\frac{g^2 \langle A^2 \rangle}{12 p^2} \times \frac{-i\not{p}}{p^2} \end{aligned} \quad (2.1)$$

where  $\langle \rangle$  represents the vacuum expectation value,  $\sum \lambda_a^2/4 = C_F = 4/3$  (proportional to the identity matrix in color space), the sum over  $\mu$  gives a factor 4, and

$$\langle (A_\mu^a)^2 \rangle = \langle A^2/32 \rangle, \quad \langle (A \cdot \hat{p})^2 \rangle = \langle A^2/4 \rangle \quad (2.2)$$

from the homogeneity of the vacuum for rotations in space-time and color space.

For  $Z_q$  defined by Eq. (1.2), we get at tree level the following non-perturbative contribution due to  $\langle A^2 \rangle$ :

$$\delta Z_q = \frac{g^2 \langle A^2 \rangle}{12 p^2} \quad (2.3)$$

### 2.2.2 The Wilson coefficients at $O(\alpha^4)$

The Wilson coefficient of  $\langle A^2 \rangle$  for the quark propagator has been computed up to  $O(\alpha^4)$  in [9] in the  $\overline{\text{MS}}$  scheme. Our lattice data refer naturally to the RI'-MOM scheme. Some work is needed to derive the correct analytic formula which allows a fitting of our lattice data. We have derived this in the appendix A.

## 3 The lattice computations

The results presented here are based on the gauge field configurations generated by the European Twisted Mass Collaboration (ETMC) with the tree-level improved Symanzik gauge action [16] and the twisted mass fermionic action [17] at maximal twist.

### 3.1 The lattice action

A very detailed discussion about the twisted mass and tree-level improved Symanzik gauge actions, and about the way they are implemented by ETMC, can be found in refs. [18–21]. Here, for the sake of completeness, we will present a brief reminder of the twisted action and the run parameters for the gauge configurations that will be exploited in the present work (See tab. 1).

The Wilson twisted mass fermionic lattice action for two flavours of mass degenerate quarks, reads (in the so called twisted basis [17, 22] )

$$S_{\text{tm}}^{\text{F}} = a^4 \sum_x \left\{ \bar{\chi}_x [D_{\text{W}} + m_0 + i\gamma_5 \tau_3 \mu_q] \chi_x \right\}, \quad (3.1)$$

$$D_{\text{W}} = \frac{1}{2} \gamma_\mu (\nabla_\mu + \nabla_\mu^*) - \frac{ar}{2} \nabla_\mu \nabla_\mu^*,$$

where  $m_0$  is the bare untwisted quark mass and  $\mu_q$  the bare twisted quark mass,  $\tau_3$  is the third Pauli matrix acting in flavour space and  $r$  is the Wilson parameter, which is set to  $r = 1$  in the simulations. The twisted Dirac operator is defined as

$$D_{\text{tw}} \equiv D_{\text{W}} + m_0 + i\gamma_5 \tau_3 \mu_q. \quad (3.2)$$

The operators  $\nabla_\mu$  and  $\nabla_\mu^*$  stand for the gauge covariant nearest neighbour forward and backward lattice derivatives:

$$\begin{aligned} \nabla_\mu(x, y) &\equiv [\delta_{y, x+\hat{\mu}} U_\mu(x) - \delta_{x, y}] , \\ \nabla_\mu^*(x, y) &= [\delta_{x, y} - \delta_{y, x-\hat{\mu}} U_\mu^\dagger(x - \hat{\mu})] , \\ D_\mu &\equiv \frac{1}{2} [\nabla_\mu(x, y) + \nabla_\mu^*(x, y)] = \frac{1}{2} [\delta_{y, x+\hat{\mu}} W(x, y) - \delta_{y, x-\hat{\mu}} W(x, y)] ; \end{aligned} \quad (3.3)$$

defining the operator  $D_\mu$  as the discretized covariant derivative. The bare quark mass  $m_0$  is related as usual to the so-called hopping parameter  $\kappa$ , by  $\kappa = 1/(8 + 2am_0)$ . Twisted mass fermions are



said to be at *maximal twist* if the bare untwisted mass is tuned to its critical value,  $m_{\text{crit}}$ . This is in practice done by setting the so-called untwisted PCAC mass to zero.

In the gauge sector the tree-level Symanzik improved gauge action (tlSym) [16] is applied. This action includes besides the plaquette term  $U_{x,\mu,\nu}^{1\times 1}$  also rectangular ( $1\times 2$ ) Wilson loops  $U_{x,\mu,\nu}^{1\times 2}$ . It reads

$$S_g = \frac{\beta}{3} \sum_x \left( b_0 \sum_{\substack{\mu,\nu=1 \\ 1\leq\mu<\nu}}^4 \{1 - \text{ReTr}(U_{x,\mu,\nu}^{1\times 1})\} + b_1 \sum_{\substack{\mu,\nu=1 \\ \mu\neq\nu}}^4 \{1 - \text{ReTr}(U_{x,\mu,\nu}^{1\times 2})\} \right), \quad (3.4)$$

where  $\beta \equiv 6/g_0^2$ ,  $g_0$  being the bare lattice coupling and it is set  $b_1 = -1/12$  (with  $b_0 = 1 - 8b_1$  as dictated by the requirement of continuum limit normalization). Note that at  $b_1 = 0$  this action becomes the usual Wilson plaquette gauge action. The run parameters for  $\beta$  and  $\mu_q$  of the gauge configurations that will be exploited in the following can be found in tab. 1.

$\beta$	$a$ fm	$a^{-1}$ GeV	$a\mu_q$	Volume	# confs
3.9	0.083	2.373	0.004	$24^3 \times 48$	100
4.05	0.0675	2.897	0.006	$24^3 \times 48$	100
4.2	0.055	3.58	0.002	$24^3 \times 48$	100

Table 1: Run parameters of the exploited data from ETMC collaboration for the present study of  $Z_q$ . The second column lists the lattice spacings which we have used in this study. It is easy to convert it to other lattice spacings.

## 3.2 The computation of the quark propagator

Computing the renormalisation constants for the quark propagator and the operators containing quark fields demands to compute first the gauge-fixed 2-point quark Green functions from the lattice. We exploited ETMC gauge configurations [23] obtained for  $\beta = 3.9$ ,  $\beta = 4.05$  and  $\beta = 4.2$ . After checking the small dependence of  $Z_q$  on the dynamical and valence quark masses we decided to use only one mass for every  $\beta$ , table 1. The lattice gauge configurations are transformed to Landau gauge by minimising the following functional of the SU(3) matrices,  $U_\mu(x)$ ,

$$F_U[g] = \text{Re} \left[ \sum_x \sum_\mu \text{Tr} \left( 1 - \frac{1}{N} g(x) U_\mu(x) g^\dagger(x + \mu) \right) \right], \quad (3.5)$$

with respect to the gauge transform  $g$ , by applying a combination of overrelaxation algorithm and Fourier acceleration <sup>3</sup>.

<sup>3</sup>We end when  $|\partial_\mu A_\mu|^2 < 10^{-11}$  and when the spatial integral of  $A_0$  is constant in time to better than  $10^{-6}$ .

We compute quark propagators with a local source taken at a random point  $x_0$  on the lattice, in order to reduce the correlation between successive configurations:

$$S(y, x_0)_j^{a, \alpha; b_0, \beta_0} = D_{\text{tw}}^{-1}(y, x)^{a, \alpha; b, \beta; i, j} sO_j^{b, \beta}(x, x_0), \quad sO_j^{b, \beta}(x, x_0) = \delta_{x, x_0} \delta_{b, b_0} \delta_{\beta, \beta_0}; \quad (3.6)$$

where the equation is solved for every  $b_0 = 1, 3$  and  $\beta_0 = 1, 4$ , and  $j = u, d$  labels the isospin. We perform the Fourier transform which is a  $12 \times 12$  complex matrix

$$S_i(p) \equiv \sum_y e^{-ip(y-x_0)} S_i(y, x_0). \quad (3.7)$$

This is the Fourier transform of the quark incoming to the source (the arrow pointing towards the source). The Fourier transforms of the quark outgoing from the source is

$$S_i^{\dagger 5}(p) = \gamma_5 S_i^\dagger(p) \gamma_5, \quad (3.8)$$

where  $\bar{u} \equiv d; \bar{d} \equiv u$ . From Eq. (1.2) the lattice quark renormalisation constant  $Z_q$  is given by

$$Z_q(p) \equiv \frac{-i}{12 \tilde{p}^2} \langle \text{Tr}[S^{-1}(p) \tilde{p}] \rangle, \quad (3.9)$$

where  $\langle \dots \rangle$  means here the average over the chosen ensemble of thermalised configurations and  $\tilde{p}_\mu = \frac{1}{a} \sin ap_\mu$ . The reason to use  $\tilde{p}_\mu = \frac{1}{a} \sin ap_\mu$  is to get  $Z_q = 1$  for a free fermion, or in other words, to eliminate hypercubic artefacts at tree level.

### 3.3 The method of non-perturbative Hypercubic $H(4)$ correction

The lattice estimates of the quark field renormalisation constant and the vertex functions lead to dimensionless quantities that, because of general dimensional arguments, depend on the strong interaction scale  $\Lambda_{\text{QCD}}$  and on the lattice momentum  $ap_\mu$ . We have computed the Fourier transforms for the following momenta:

$$p_i = \frac{2\pi n_i}{N_L a} \quad n_i = -N_L/4, \dots, N_L/4, \quad p_4 = \frac{\pi(2n_4 + 1)}{N_T a} \quad n_4 = -N_T/4, \dots, N_T/4; \quad (3.10)$$

where  $p_i = 1, 3$  are the spatial momenta and  $p_4$  the time like. The antiperiodic boundary condition in the time direction explains the  $\pi(2n_4 + 1)$  factor.

The lattice action Eq. (3.1) and Eq. (3.4) is invariant under the hypercubic group  $H(4)$ . However the boundary conditions and the difference between the spatial size  $N_L$  and the time-like one  $N_T = 2N_L$  generate finite volume corrections to the hypercubic symmetry. Only the cubic symmetry is exact. We define cubic invariant quantities and compute their average over the cubic group. We have thus a set of measures for every orbit of the cubic group, labelled by

$$\left( \sum_{i=1,3} p_i^m, p_4 \right), \quad (3.11)$$

where  $m = 2, 4, 6$ .

A first kind of artefacts that can be systematically cured [12,24,25] are those due to the breaking of the rotational symmetry of the Euclidean space-time when using an hypercubic lattice, where this symmetry is restricted to the discrete hypercubic  $H(4)$  isometry group. However, as already mentioned, we have also finite volume effects which break  $H(4)$ . We therefore need to adapt the method. One idea could be to generalise it to a cubic symmetry. This happens not to be practical due to too few cubic symmetric orbits for a given  $\vec{p}^2$ . We choose another approach motivated by the fact that the lattice action is indeed  $H(4)$  symmetric and that finite volume effects are expected to be small at large momenta compared to finite lattice spacing artefacts. We therefore use a slight variation of the method described in [24,25] : *we apply it to the cubic orbits of Eq. (3.11)*, keeping track of  $p_4$  which is not an  $H(4)$  symmetric quantity.

Defining the  $H(4)$  invariants

$$p^{[4]} = \sum_{\mu=1}^4 p_{\mu}^4, \quad p^{[6]} = \sum_{\mu=1}^4 p_{\mu}^6, \quad p^{[8]} = \sum_{\mu=1}^4 p_{\mu}^8; \quad (3.12)$$

it happens that every cubic orbit Eq. (3.11) has a well defined set of values for these  $H(4)$  invariants, but several cubic orbits may have the same  $H(4)$  invariants. We will neglect  $p^{[8]}$  which plays no role on small lattices. We can thus define the quantity  $Z_q(ap_{\mu})$  averaged over the cubic orbits as

$$Z_q^{\text{latt}}(a^2 p^2, a^4 p^{[4]}, a^6 p^{[6]}, ap_4, a^2 \Lambda_{\text{QCD}}^2). \quad (3.13)$$

We expect the hypercubic effects to be  $O(a^2)$  lattice artefacts and therefore to be expandable into powers of  $a^2$ . This would of course trivially be the case if  $a^2 p^2 \ll 1$  since then, for example  $\epsilon = a^2 p^{[4]}/p^2 \leq a^2 p^2 \ll 1$  (we take on purpose this quantity which will be seen to be dominant). Then a Taylor expansion of Eq. (3.13) will ensure the artefact to be  $O(a^2)$ . However, aiming at measuring  $Z_q$  at large momentum we go up to  $a^2 p^2 \sim 3 - 4$ . We will assume, and then check, that the  $Z_q^{\text{latt}}$  in Eq. (3.13) can be Taylor-expanded around  $p^{[4]} = 0$  up to  $\epsilon$  significantly larger than 1:

$$\begin{aligned} Z_q^{\text{latt}}(a^2 p^2, a^4 p^{[4]}, a^6 p^{[6]}, ap_4, a^2 \Lambda_{\text{QCD}}^2) &= Z_q^{\text{hyp-corrected}}(a^2 p^2, ap_4, a^2 \Lambda_{\text{QCD}}^2) \\ &+ R(a^2 p^2, a^2 \Lambda_{\text{QCD}}^2) a^2 \frac{p^{[4]}}{p^2} + \dots \end{aligned} \quad (3.14)$$

where

$$R(a^2 p^2, a^2 \Lambda_{\text{QCD}}^2) = \left. \frac{dZ_q^{\text{latt}}(a^2 p^2, 0, 0, 0, a^2 \Lambda_{\text{QCD}}^2)}{d\epsilon} \right|_{\epsilon=0}. \quad (3.15)$$

Of course terms proportional to  $p^{[6]}$ ,  $p^{[4]^2}$ , etc. can be added analogously to the formula, as well as terms breaking  $H(4)$ . However we have found that our data were not accurate enough to allow fitting them, and that using only Eq. (3.14) and Eq. (3.15) gave satisfactory fits. Now we must describe how we fit the functions appearing in the r.h.s of Eq. (3.14).

### 3.3.1 The sliding window fit (SWF)

We consider all values of  $a^2 p^2$  in a range:  $a^2 p_{\min, \text{in}}^2 \leq a^2 p^2 \leq a^2 p_{\max, \text{in}}^2$ , each of which contains a set of cubic orbits. We choose an integer width  $w$  (we will use  $w = 10$  in numerical applications) and define a window as the set of  $2w + 1$  values of  $a^2 p^2$  around a  $a^2 p_{\text{center}}^2$  ( $w$  contiguous values below  $a^2 p_{\text{center}}^2$  and as many above). There are as many windows as values of  $a^2 p_{\text{center}}^2$  such that all of them are in the range  $[a^2 p_{\min, \text{in}}^2, a^2 p_{\max, \text{in}}^2]$ . This defines the range of interest  $a^2 p_{\min, \text{out}}^2 \leq a^2 p_{\text{center}}^2 \leq a^2 p_{\max, \text{out}}^2$ .

For every window we use for the fit all cubic orbits corresponding to the values of  $a^2 p^2$  in the window. We fit, according to Eq. (3.14),  $2w + 2$  parameters which are the  $2w + 1$  values of  $Z_q^{\text{hyp-corrected}}(a^2 p^2, a^2 \Lambda_{\text{QCD}}^2)$  within the window, and one common value of  $R(a^2 p_{\text{center}}^2, a^2 \Lambda_{\text{QCD}}^2)$ . The dependence in these parameters is linear and thus the fit amounts to invert a matrix. It is clear that for any  $a^2 p^2$  the  $Z_q^{\text{hyp-corrected}}(a^2 p^2, a^2 \Lambda_{\text{QCD}}^2)$  is fitted every time  $a^2 p^2$  is within a window, i.e.  $2w + 1$  times. We keep as the final result only the result of the fit when  $a^2 p^2$  is the center of the window. At the end of the fit, for every  $a^2 p_{\text{center}}^2$  in the range  $a^2 p_{\min, \text{out}}^2 \leq a^2 p_{\text{center}}^2 \leq a^2 p_{\max, \text{out}}^2$  we have, as expected, a fitted value for both functions of the r.h.s of Eq. (3.14).

We can then study the function  $R(a^2 p^2, a^2 \Lambda_{\text{QCD}}^2)$ . As will be reported later (see for instance Fig. 4) we find that a reasonable approximation for  $R$  is

$$R(a^2 p^2, a^2 \Lambda_{\text{QCD}}^2) = c_{a^2 p^4} + c_{a^4 p^4} a^2 p^2 . \quad (3.16)$$

This leads to the one window fit.

### 3.3.2 The one window fit (OWF)

We tune  $w$  such that only one (or at worst two) windows are included in the range  $[a^2 p_{\min, \text{in}}^2, a^2 p_{\max, \text{in}}^2]$ . We then perform the fit for that window according to the equation

$$\begin{aligned} Z_q^{\text{latt}}(a^2 p^2, a^4 p^{[4]}, a^6 p^{[6]}, a p_4, a^2 \Lambda_{\text{QCD}}^2) &= Z_q^{\text{hyp-corrected}}(a^2 p^2, a^2 \Lambda_{\text{QCD}}^2) + c_{a^2 p^4} a^2 \frac{p^{[4]}}{p^2} \\ &+ c_{a^4 p^4} a^4 p^{[4]} . \end{aligned} \quad (3.17)$$

This fit gives  $2w + 3$  parameters which are  $Z_q^{\text{hyp-corrected}}(a^2 p^2, a^2 \Lambda_{\text{QCD}}^2)$  for all  $a^2 p^2$  in the window, i.e. in the range  $[a^2 p_{\min, \text{in}}^2, a^2 p_{\max, \text{in}}^2]$ , (or if the range size is even one value is eliminated) and the parameters  $c_{a^2 p^4}$  and  $c_{a^4 p^4}$ .

## 3.4 Other lattice artefacts

There are ultraviolet artefacts which are functions of  $a^2 p^2$  and are thus insensitive to hypercubic biases and not corrected by the above-mentioned method. They will be corrected simply by assuming a term linear in  $a^2 p^2$  in the final fit and check that the coefficient scales correctly for different lattice spacings.

To take into account the space-time anisotropy, which is a finite volume artefact, we can check the dependence of  $Z_q$  on an anisotropic quantity such as  $p_4^2 - \vec{p}^2/3$ . We did not see any sizeable effect of this parameter.

Finite volume artefacts are also studied as usual by a comparison of runs at different volume. We expect a small effect at large momenta and our checks confirmed it, as well as the analysis of [7]. We will not consider this artefact anymore.

## 4 Lattice results and hypercubic corrections

The hypercubic artefacts generate on the raw lattice data,  $Z_q^{\text{latt}}$ , the so called “half-fishbone” structure [12] shown in fig 1. In this figure all the points labelled as explained in Eq. (3.10) and Eq. (3.11) are plotted. The color code shows the value of the ratio  $p^{[4]}/(p^2)^2$  which is between 0.25 and 1. The closer to 1 means the less “democratic” or “tyrannic” ones. We see, as expected, that the tyrannic points are more affected by the artefacts. We also see that the gap between  $Z_q^{\text{latt}}(a^2 p^2, a^4 p^{[4]}, a^6 p^{[6]}, ap_4, a^2 \Lambda_{\text{QCD}}^2)$  at a given  $p^2$  can be as large as 0.07, i.e; about 10%. Taking a naive average, without a correct treatment of this artefact would leave a systematic upward shift of about 5 %. In section 3.3 we have developed a non-perturbative method to cure this artefact (this method being indeed splitted in two options, the SWF and the OWF). There exist two other methods. The oldest one is the “democratic selection”. It amounts to keep only, say, the points with ratio  $\leq 0.3$  in fig 1. One sees that it eliminates a lot of data and it is still far from the “egalitarian” result (the lowest curve in fig 1) which we consider as better. We will thus not consider further this democratic selection. The second other method to correct hypercubic artefacts uses perturbative calculation and is detailed in the next section.

### 4.1 Perturbative correction

The perturbative method [26] consists in computing at one loop in lattice perturbation theory [27], then, assuming that the lattice spacing artefacts are reliably described by the  $O(g^2 a^2)$  terms thus obtained, in subtracting them from the lattice data. This method has been applied to quark bilinear operators in [28]. For comparison we have applied here this method following the prescription described in section 3.2.2 of [28] and also a variant of it.

Eq (24) in [26] may be written in Landau gauge as

$$Z_q^{\text{pert}}(a^2 p^2) = Z_q^{\text{tree}}(a^2 p^2) + \tilde{g}^2 (b_{q1} + c_{q1} a^2 p^2 + c_{q2} a^2 p^2 \log(a^2 p^2) + c_{q3} \frac{a^2 p^{[4]}}{p^2} + c_{q4} \frac{a^2 p^{[4]}}{p^2} \log(a^2 p^2)) , \quad (4.1)$$

where, to follow [28],  $\tilde{g}^2 = g_{\text{boosted}}^2/(12\pi^2)$ , with  $g_{\text{boosted}}^2 = g_{\text{bare}}^2/\langle \text{plaquette} \rangle$ . The coefficients

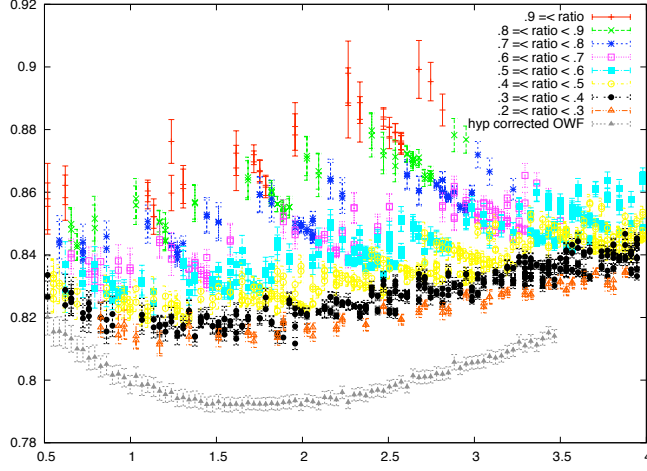


Figure 1: This plot shows the raw data for  $\beta = 3.9$ ,  $Z_q^{\text{latt}}(a^2 p^2, a^4 p^{[4]}, a^6 p^{[6]}, ap_4, a^2 \Lambda_{\text{QCD}}^2)$  in Eq. (3.14), in terms of  $a^2 p^2$  in the horizontal axis. The “half-fishbone structure” due to hypercubic artefacts is clearly seen. There is one point for every cubic (3-D) orbit. The color code classifies the data according to their degree of “democracy” measured by  $\text{ratio} = p^{[4]}/(p^2)^2$ . The lowest plot corresponds to the non-perturbatively hypercubic corrected data (or “egalitarian result”) resulting from the one-window fit  $Z_q^{\text{hyp.corrected}}(a^2 p^2, a^2 \Lambda_{\text{QCD}}^2)$  in Eq. (3.17). The data correspond to  $\beta = 3.9, a\mu = 0.004$ , but the same features appear for all  $\beta$ 's.

are defined using the notations of eq. (24) in [26]:

$$c_{q1} = \epsilon^{(2,4)} , \quad c_{q2} = \frac{59}{240} + \frac{c_1}{2} + \frac{C_2}{60} ,$$

$$c_{q3} = \epsilon^{(2,1)} - \frac{3}{80} - \frac{C_2}{10} , \quad c_{q4} = \frac{101}{120} - \frac{11}{30} C_2 .$$

#### 4.1.1 Prescription with $\tilde{p}_\mu$

Using the prescription of eq. (35) in [28], for every cubic orbit we define the substracted quantity as :

$$Z_q^{\text{pert.tilde}}(a^2 p^2, a^4 p^{[4]}, a^6 p^{[6]}, ap_4, a^2 \Lambda_{\text{QCD}}^2) = Z_q^{\text{latt}}(a^2 p^2, a^4 p^{[4]}, a^6 p^{[6]}, ap_4, a^2 \Lambda_{\text{QCD}}^2) - \tilde{g}^2 \left( c_{q1} a^2 \tilde{p}^2 + c_{q2} a^2 \tilde{p}^2 \log(a^2 \tilde{p}^2) + c_{q3} \frac{a^2 \tilde{p}^{[4]}}{\tilde{p}^2} + c_{q4} \frac{a^2 \tilde{p}^{[4]}}{\tilde{p}^2} \log(a^2 \tilde{p}^2) \right) \quad (4.2)$$

The result of this substraction is plotted in the l.h.s of fig. 2. The half-fishbone structure is still clearly visible for  $a^2 p^2 > 1.6$ . We then try another prescription.

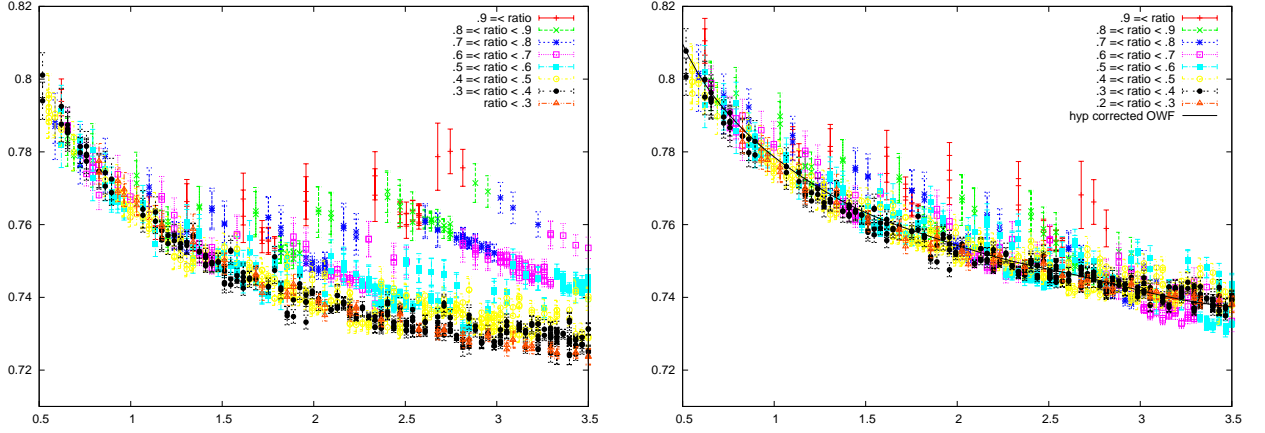


Figure 2: L.h.s: data of fig. 1 corrected by the perturbative subtraction, formula of Eq. (4.2), section 4.1.1. R.h.s: same exercise with the prescription Eq. (4.3) with Eq. (4.2). The color code is the same as in fig 1 and ratio =  $p^{[4]}/(p^2)^2$ . The horizontal axis is  $a^2 p^2$  for both.

#### 4.1.2 Prescription with $p_\mu$

The trace of Eq. (3.9), which introduces  $\tilde{p}_\mu$ , had to be applied in eq. (24) of [26] to obtain Eq. (4.1). We will now expand in  $p_\mu$  before performing the trace and then keep the  $O(g^2 a^2)$  terms for subtraction. This gives, using again [26],

$$Z_q^{\text{pert\_notilde}}(a^2 p^2, a^4 p^{[4]}, a^6 p^{[6]}, ap_4, a^2 \Lambda_{\text{QCD}}^2) = Z_q^{\text{latt}}(a^2 p^2, a^4 p^{[4]}, a^6 p^{[6]}, ap_4, a^2 \Lambda_{\text{QCD}}^2) - \tilde{g}^2 \left( c_{q1} a^2 p^2 + c_{q2} a^2 p \log(a^2 p^2) + c'_{q3} \frac{a^2 p^{[4]}}{p^2} + c_{q4} \frac{a^2 p^{[4]}}{p^2} \log(a^2 p^2) \right), \quad (4.3)$$

where

$$c'_{q3} = \frac{\epsilon^{(0,1)}}{6} + \epsilon^{(2,1)} - \frac{3}{80} - \frac{C_2}{10} = c_{q3} + \frac{\epsilon^{(0,1)}}{6}. \quad (4.4)$$

This result is plotted in the r.h.s. of fig. 2. With this variant, the half-fishbone is significantly reduced but the dominant  $O(4)$  artefact is overcorrected : a linear behaviour in  $a^2 p^2$  is clearly visible, larger than with the first prescription.

#### 4.1.3 Lessons about the perturbative method

We see that the two prescriptions start differing significantly at  $a^2 p^2 \simeq 1$ , which is not surprising since higher order terms become significant, for example, an  $a^4 p^{[4]}$  is also of order 1 for tyrannic

points, while  $a^2 p^2 - a^2 \tilde{p}^2 \simeq 0.3$ . The perturbative method goes in the right direction, but it is impossible to know a priori its quality without performing the tests we propose here. The method contains several ambiguities: what to take for the coupling constant ? use  $p_\mu$  or  $\tilde{p}_\mu$ ? Contrarily to the non-perturbative method it provides both the hypercubic corrections and the  $O(a^2 p^2)$  ones. Conceptually the perturbative method is very useful as it exhibits qualitative aspects which may guide the use of the non-perturbative one, for example it justifies the smoothness of the variation of the derivative  $R$  Eq. (3.15) as a function of  $a^2 p^2$  as well as that of the slope in  $a^2 p^2$ . Finally we shall see that it gives results similar to the non-perturbative ones.

## 4.2 Non perturbative hypercubic correction

### 4.2.1 Sliding window fit versus one window fit

We now apply the non-perturbative correction. We only expand in  $p^{[4]}$  since the higher order terms turn out to be negligible in our momentum range. In section 3.3 we have presented two types of fits, similar in spirit: the sliding window fit (SWF) described in section 3.3.1 which amounts to using Eq. (3.14) combined with Eq. (3.15) and the one window fit (OWF) described in section 3.3.2 which amounts to using Eq. (3.16). In the l.h.s of Fig. 3 we show, in the case of  $\beta = 3.9$ , the comparison of hypercubic corrected data after applying OWF and SWF. The difference does not appear to be large which is rather encouraging. The OWF gives a slightly smoother result. For this value of  $\beta$  the chi-squared is not good (see table 2) but remember it uses only two hypercubic parameters. Chi-squared for the other  $\beta$ 's are better.

### 4.2.2 Half-fishbone reduction test

We need also to apply the half-fishbone reduction test as in the perturbative case, i.e. to subtract to the raw data of every cubic orbit the hypercubic correction. We present the OWF result. From Eq. (3.17) the subtraction amounts to

$$\begin{aligned} Z_q^{\text{non-pert.OWF}}(a^2 p^2, a^4 p^{[4]}, a^6 p^{[6]}, ap_4, a^2 \Lambda_{\text{QCD}}^2) &= Z_q^{\text{latt}}(a^2 p^2, a^4 p^{[4]}, a^6 p^{[6]}, ap_4, a^2 \Lambda_{\text{QCD}}^2) \\ &- c_{a2p4} a^2 \frac{p^{[4]}}{p^2} - c_{a4p4} a^4 p^{[4]} \end{aligned} \quad (4.5)$$

The result is shown in the r.h.s of Fig. 3, one point per cubic orbit. The non-perturbatively corrected  $Z_q^{\text{hyp-corrected}}(a^2 p^2, a^2 \Lambda_{\text{QCD}}^2)$  of Eq. (3.17) is represented by the black line in the r.h.s of Fig. 3. It is well in the middle of the subtracted points, as we would expect.

It is seen that the half-fishbones have been strongly reduced. One sees a remainder of these artefacts due to the less democratic, or ‘‘tyrannic’’ points. These have only one non-vanishing component or one large and a very small one. These points are not so many as seen in the plot, their orbits are small which explains the larger error bars.

We have checked that these tyrannic points have indeed a small impact on the hypercubic corrected result.



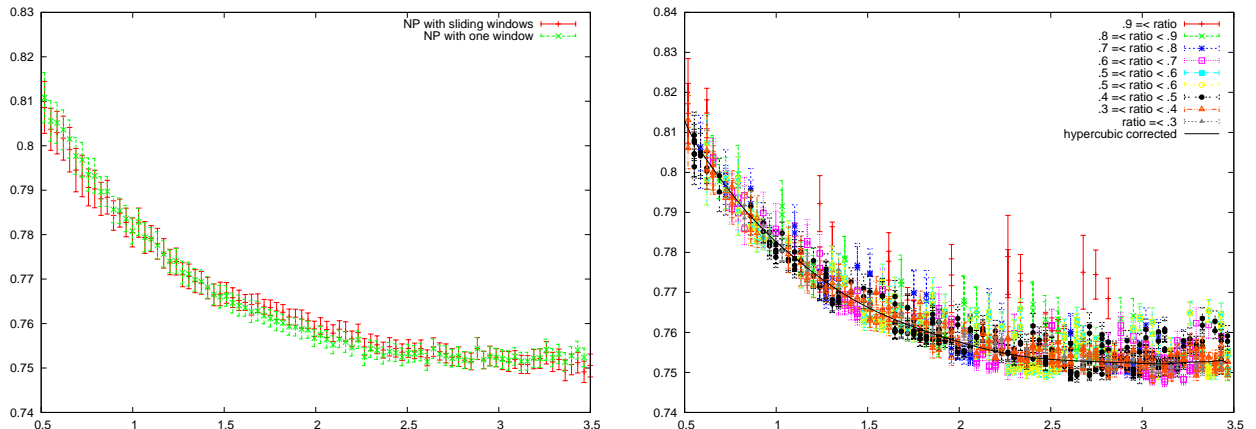


Figure 3: On the l.h.s we compare for  $\beta = 3.9, a\mu = 0.004$  the non-perturbatively corrected  $Z_q$  from the sliding-window fit (SWF), section 3.3.1 and from the one-window one (OWF), section 3.3.2. To show better the running we have also subtracted the  $O(a^2 p^2)$  artefact which will be computed below. On the r.h.s we show, using the OWF, the non-perturbatively subtracted data Eq. (4.5). There is one point for every cubic (3-D) orbit. The color code and the definition of the parameter ratio are the same as in fig. 1. The black line corresponds to the OWF non-perturbatively corrected result:  $Z_q^{\text{hyp-corrected}}(a^2 p^2, a^2 \Lambda_{\text{QCD}}^2)$  of Eq. (3.17). The  $O(a^2 p^2)$  has also been subtracted. The horizontal axis is  $a^2 p^2$ .

#### 4.2.3 The slopes in $p^{[4]}$

The sliding window fit solves for every window a value for the slope  $R(a^2 p^2)$  Eq. (3.15), i.e. the derivative  $\partial Z_q^{\text{latt}} / \partial(a^2 p^{[4]} / p^2)$ . This allows for a study of the shape of this function  $R$ . In Fig. 4 we plot this slope  $R$  defined in Eq. (3.15) for the three values of  $\beta$ . We also plot the equivalent slope using the perturbative formula with the  $p_\mu$  prescription for  $\beta = 3.9$ , section 4.1.2:  $R_{\text{pert}} = c'_{q3} + c_{q4} \log(a^2 p^2)$ ,  $c'_{q3}$  defined in Eq. (4.4) and  $c_{q4}$  in Eq. (4.2). We see that this perturbative slope is in fair agreement with the non-perturbative one, explaining the good elimination of half-fishbones in the r.h.s. in Fig. 2.

The three non-perturbative data in Fig. 4 give the impression to be affine (a constant minus a linear term) over a rather large momentum interval. This is what is expressed in Eq. (3.16) from where we have deduced the one-window fit: a fit over the full range [0.5-3.5] with two hypercubic parameters only <sup>4</sup>

The fitted values for  $c_{a2p4}$  and  $c_{a4p4}$  from the one window fit are given in table 2 as well as the same divided by  $g^2$ , since perturbation theory expects at least for  $c_{a2p4}$  to be  $\propto g^2$ . Before

<sup>4</sup>Of course there are additionally as many hypercubic insensitive parameters as there are values of  $p^2$  in the range, which are simply the values of  $Z_q^{\text{hyp-corrected}}(a^2 p^2, a^2 \Lambda_{\text{QCD}}^2)$ .

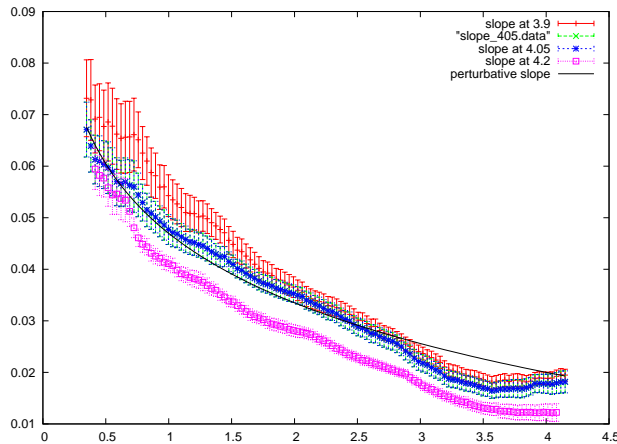


Figure 4: The three lattice slopes  $R$  defined in Eq. (3.15) for the three lattice spacings and the perturbative one  $R_{\text{pert}} = c'_{q3} + c_{q4} \log(a^2 p^2)$  for  $\beta = 3.9$ , in terms of  $a^2 p^2$  in the horizontal axis.

$\beta$	$a^2 \text{ fm}^2$	$c_{a2p4}$	$c_{a4p4}$	$c_{a2p4}/g^2$	$c_{a4p4}/g^2$	$\chi^2/\text{d.o.f}$
3.9	0.00689	0.067(4)	-0.0149(10)	0.044(3)	-0.0097(7)	4.1
4.05	0.00456	0.065(3)	-0.0144(5)	0.044(2)	-0.0097(3)	0.53
4.2	0.00303	0.055(11)	-0.0124(4)	0.039(8)	-0.0089(3)	0.98

Table 2: Results for the slope in  $a^2 p^{[4]}/p^2$  and  $a^4 p^{[4]}$  and the same divided by  $g^2$  in the one window fit.

dividing by  $g^2$  a small scaling violation is apparent, which corresponds to the non overlap of the curves at different  $\beta$ 's in Fig. 4 It appears on table 2 that dividing by  $g^2$  improves significantly the scaling. The  $\chi^2$  in table 2 is not good for  $\beta = 3.9$ , apparently due to some structure at the lower end of the plot.

## 5 Running including $\langle A^2 \rangle$ corrections from OPE

In this section we will check the running of  $Z_q$ . To this purpose, we shall use both the formula Eq. (A.24) derived in the appendix A, to which we add a lattice artefact term  $\propto a^2 p^2$  not yet

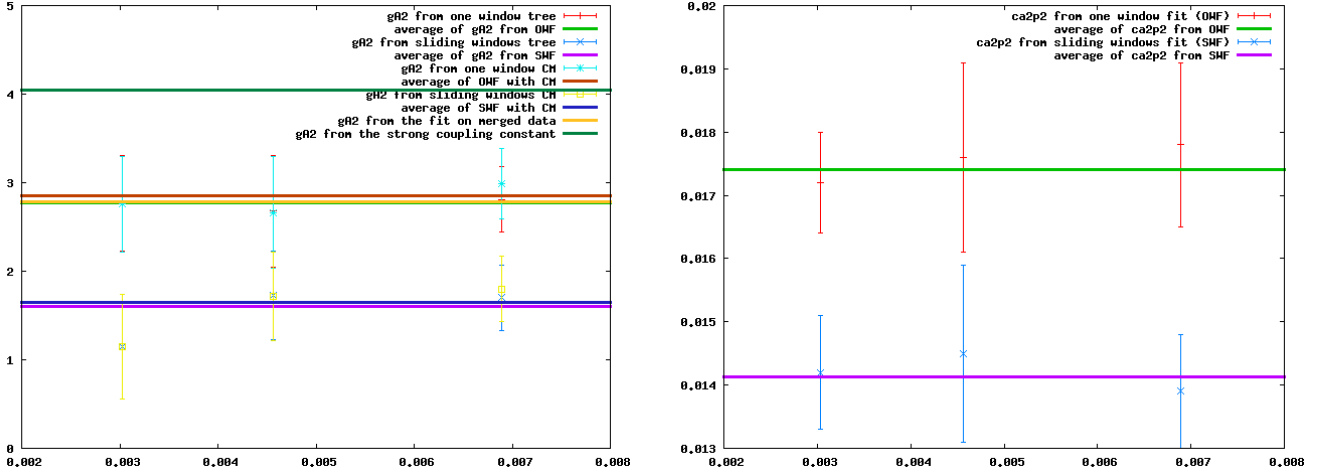


Figure 5: We plot the values of the fitted slopes  $c_{a2p2}$  (r.h.s) and the condensate  $g^2 \langle A^2 \rangle$  (l.h.s) as extracted from the  $1/p^2$  contribution to the fit, see table 3, 4 and 7. In the left plot we show the results from the OWF and from the SWF. It can be seen that the  $O(\alpha^4)$  formula for the Wilson coefficient computed by Chetyrkin and Maier [9] of  $\langle A^2 \rangle$  (indicated by the "CM" initials) is about 20 % below the tree level result. We show the value obtained from the merged results of the three lattice spacings, table 7. Finally, for the sake of comparison we show the result from the strong coupling constant of [7]. The horizontal axis is  $a^2$  in  $\text{fm}^2$ .

subtracted:

$$\begin{aligned}
Z_q^{\text{hyp-corrected}}(a^2 p^2) &= Z_q^{\text{pert RI}'}(\mu'^2) c_{0Z_q}^{\text{RI}'}\left(\frac{p^2}{\mu'^2}, \alpha(\mu')\right) \\
&\times \left( 1 + \frac{c_{2Z_q}^{\overline{\text{MS}}}\left(\frac{p^2}{\mu^2}, \alpha(\mu)\right)}{c_{0Z_q}^{\text{RI}'}\left(\frac{p^2}{\mu^2}, \alpha(\mu)\right)} \frac{c_{2Z_q}^{\text{RI}'}\left(\frac{p^2}{\mu^2}, \alpha(\mu)\right)}{c_{2Z_q}^{\overline{\text{MS}}}\left(\frac{p^2}{\mu^2}, \alpha(\mu)\right)} \frac{\langle A^2 \rangle_{R, \mu^2}}{32 p^2} \right) \\
&+ c_{a2p2} a^2 p^2 .
\end{aligned} \tag{5.1}$$

and a formula including only an OPE correction with a tree-level Wilson coefficient,

$$Z_q^{\text{hyp-corrected}}(a^2 p^2) = Z_q^{\text{pert RI}'}(\mu'^2) c_{0Z_q}^{\text{RI}'}\left(\frac{p^2}{\mu'^2}, \alpha(\mu')\right) \left( 1 + \frac{c_{1overp2}}{p^2} \right) + c_{a2p2} a^2 p^2 , \tag{5.2}$$

where  $c_{1overp2} = g^2 \langle A^2 \rangle / 12$ . We use  $\mu' = \mu = 10 \text{ GeV}$  as the renormalisation scale ;  $c_{0Z_q}^{\text{RI}'}(p^2, \mu^2)$  is computed from the four loop perturbative running of  $Z_q$  [13]:

$$c_{0Z_q}^{\text{RI}'}(p^2, \mu^2) \equiv \frac{Z_q^{\text{pert RI}'}(p^2, g_{\text{bare}}^2)}{Z_q^{\text{pert RI}'}(\mu^2, g_{\text{bare}}^2)} ; \tag{5.3}$$

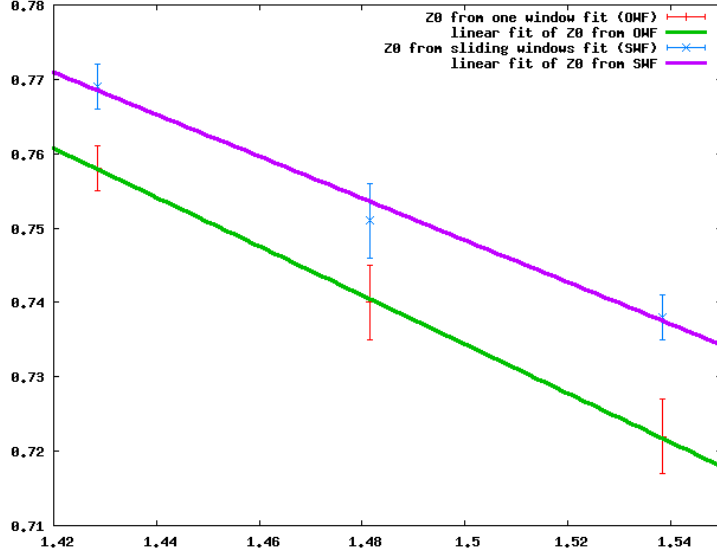


Figure 6: We show the value of  $Z_q^{\text{pert}}$  defined in Eq. (5.1) for all three lattice spacings as a function of the bare coupling constant  $g^2 = 6/\beta$ .

$\overline{c_{2Z_q}^{\text{MS}}}(p^2, \mu^2)$  is the three loop Wilson coefficient of  $\langle A^2 \rangle$  in the expansion of  $Z_q$  [9] and the ratio

$$\frac{c_{2Z_q}^{\text{RI}'}\left(\frac{p^2}{\mu^2}, \alpha(\mu)\right)}{\overline{c_{2Z_q}^{\text{MS}}}\left(\frac{p^2}{\mu^2}, \alpha(\mu)\right)} = \frac{1 - 0.1317 \alpha^2(\mu) - 0.5155 \alpha^3(\mu)}{1 - 0.1317 \alpha^2(p) - 0.5155 \alpha^3(p)} \quad (5.4)$$

was obtained in appendix A. We express the lattice spacing (cut-off) dependence as a dependence in  $g_{\text{bare}}^2$ .  $Z_q^{\text{pert RI}'}(\mu^2, g_{\text{bare}}^2)$  is the perturbative contribution to  $Z_q$  at the scale  $\mu$  in the RI'-MOM scheme. In other words,

$$\begin{aligned} Z_q^{\text{RI}'}(p^2, g_{\text{bare}}^2) &= Z_q^{\text{pert RI}'}(p^2, g_{\text{bare}}^2) \\ &\times \left( 1 + \frac{\overline{c_{2Z_q}^{\text{MS}}}\left(\frac{p^2}{\mu^2}, \alpha(\mu)\right)}{c_{0Z_q}^{\text{RI}'}\left(\frac{p^2}{\mu^2}, \alpha(\mu)\right)} \frac{c_{2Z_q}^{\text{RI}'}\left(\frac{p^2}{\mu^2}, \alpha(\mu)\right)}{\overline{c_{2Z_q}^{\text{MS}}}\left(\frac{p^2}{\mu^2}, \alpha(\mu)\right)} \frac{\langle A^2 \rangle_{R, \mu^2}}{32 p^2} \right) \end{aligned} \quad (5.5)$$

From now on  $Z_q^{\text{pert}}$  will refer to  $Z_q^{\text{pert RI}'}$ . We fit three parameters:  $Z_q^{\text{pert}}$ ,  $c_{a2p2}$  and alternatively  $c_{1\text{over}p2}$  (which amounts to a tree level treatment of the  $c_{2Z_q}$  coefficient) or the vev  $g^2 \langle A^2 \rangle$ . In order to estimate the systematic errors we will treat in parallel the one window fit and the sliding window one. The results are reported in table 3, table 4, Fig. 5 and Fig. 6. The coefficient  $c_{a2p2}$  obviously refers to an  $O(4)$  invariant lattice spacing artefact which is not detected by our non-perturbative

$\beta$	$a^2 \text{ fm}^2$	$Z_q^{\text{pert}}$	$c_{a2p2}$	$g^2 \langle A^2 \rangle_{\text{tree}}$	$g^2 \langle A^2 \rangle_{\text{CM}}$
3.9	0.00689	0.726(5)	0.0201(13)	3.20(38)	2.62(31)
4.05	0.00456	0.742(5)	0.0200(15)	3.09(65)	2.57(54)
4.2	0.00303	0.760(3)	0.0194(8)	3.23(55)	2.74(47)
average			0.0201(3)	3.18(28)	2.64(23)

Table 3: Results for  $Z_q^{\text{pert}}$  (10GeV) and  $c_{a2p2}$  Eq. (5.1) from the one-window-fit and the estimated  $g^2 \langle A^2 \rangle$  vev from the  $1/p^2$  term and from the the Chetyrkin-Maier [9] (CM) Wilson coefficient. Notice that  $Z_q^{\text{pert}}$  and  $c_{a2p2}$  from these two fits are very close.

$\beta$	$a^2 \text{ fm}^2$	$Z_q^{\text{pert}}$	$c_{a2p2}$	$g^2 \langle A^2 \rangle_{\text{tree}}$	$g^2 \langle A^2 \rangle_{\text{CM}}$
3.9	0.00689	0.741(3)	0.0161(9)	2.07(37)	1.70(31)
4.05	0.00456	0.753(5)	0.0168(14)	2.13(52)	1.78(43)
4.2	0.00303	0.771(3)	0.0164(9)	1.59(60)	1.36(51)
average			0.0165(6)	1.99(26)(27)	1.65(22)(27)

Table 4: The same as in table 3 using the data from the sliding-windows-fit to hypercubic corrections.

hypercubic correction method. We see in the right plot of fig. 5 as well as in the tables that this coefficient scales very well when expressed in lattice units, as it should be. The coefficient of  $1/p^2$ , if it is related to a vev  $\langle A^2 \rangle$ , should rather scale in physical units. We see in the left plot of fig. 5 that a constant value is rather well verified although with large errors. The results presented in table 3 and 4 show that the estimates for  $g^2 \langle A^2 \rangle$  from OPE expressions with Wilson coefficient from the Chetyrkin-Maier (CM) three-loop expression are systematically about 20% below the ones from the tree level one.

## 5.1 Analysis from the non-perturbative hypercubic corrections

### 5.1.1 Comparison of the running from the OWF and the SWF

From tables 3 and 4 we see that  $g^2 \langle A^2 \rangle$  is systematically larger for the OWF than for the SWF. At first sight it seems surprising since the OWF and SWF hypercubic corrected data are very similar, see Fig. 3. One reason is the correlation between  $c_{a2p2}$  and  $g^2 \langle A^2 \rangle$ :  $c_{a2p2}$  is also systematically larger for the OWF than for the SWF. This correlation is understandable as the  $a^2 p^2$  increases with  $p^2$  while  $1/p^2$  decreases. This is compensated by a  $Z_q^{\text{pert}}$  smaller for the OWF than for the SWF. We will consider these differences as a systematic uncertainty in our fits and count them in the errors.

### 5.1.2 Dependence on the fitting range

An additional test is to look for the effect of the fitting range. The results are shown in table 5 and Fig. 7. One sees again a correlation between the  $c_{a2p2}$  slope and  $g^2 \langle A^2 \rangle$ . Both decrease when

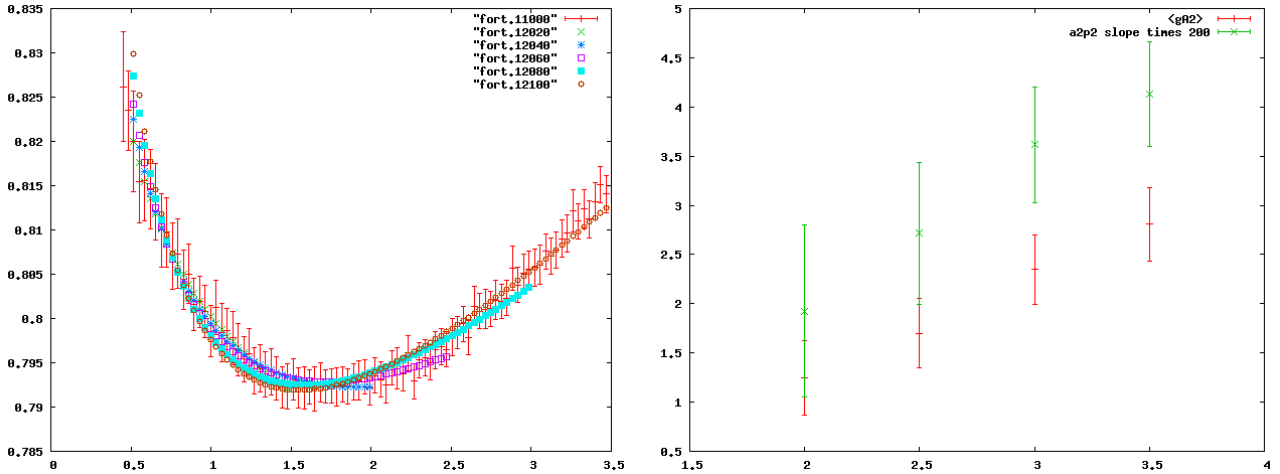


Figure 7: In the r.h.s plot we show how  $g^2 \langle A^2 \rangle$ , fitted with the CM Wilson coefficient, depends on the upper range of our fits, always starting at  $a^2 p^2 = 0.5$  for  $\beta = 3.9$ . The points correspond to  $a^2 p^2 < 2.0, 2.5, 3.0, 3.5$ . The r.h.s plot also shows the  $a^2 p^2$  artefact slope. We find again a positive correlation between both series of data. The l.h.s of the plot illustrates this, showing for the same data how the fitting function depends on the upper bound of the range.

the fitting range shortens while correlatively  $Z_q^{\text{pert}}$  increases. The l.h.s of Fig. 7 explains how this happens: when the range is shorter, the error bars allow for a less curved fit. But never the fit reaches a value such that  $g^2 \langle A^2 \rangle$  disappears. The shortest window  $0.5 < a^2 p^2 < 2.0$  gives the smallest value for  $g^2 \langle A^2 \rangle$  but still 4 sigmas away from 0.

## 5.2 Analysis from the perturbative hypercubic corrections

It is then useful to check if similar results are obtained after a perturbative correction to the hypercubic artefacts has been applied. We have used two prescriptions to apply the perturbative corrections. With the data obtained from the  $\tilde{p}_\mu$  prescription, section 4.1.1, we perform an average on all the cubic orbits of every  $p^2$  after a democratic selection  $p^{[4]}/(p^2)^2 < 0.3$ . This leaves us with not too many points and it results in rather large statistical errors. We then perform the same running fit than on the non-perturbatively hypercubic corrected results: we fit with one perturbative running contribution, one  $1/p^2$  contribution and one  $\propto a^2 p^2$  artefact. With the data from the  $p_\mu$  prescription, section 4.1.2, we perform the same fit over an average on all the cubic orbits of every  $p^2$  without any democratic selection, since the hypercubic artefacts have already been efficiently reduced. The results are in table 6.

A first remark is that the  $c_{a2p2}$  coefficients are compatible with zero, indicating that the perturbative correction has efficiently eliminated this artefact. The coefficient of the  $1/p^2$  non-perturbative contribution is found different from zero, in the same ballpark as the results from

Upper bound	$Z_q^{\text{pert}}$	$c_{a2p2}$	$g^2 \langle A^2 \rangle_{\text{tree}}$	$g^2 \langle A^2 \rangle_{CM}$
2.0	0.754(6)	0.0089(21)	1.58(39)	1.28(32)
2.5	0.745(6)	0.0130(18)	2.05(37)	1.67(30)
3.0	0.733(5)	0.0175(15)	2.73(36)	2.22(30)
3.5	0.726(5)	0.0201(13)	3.20(38)	2.62(31)

Table 5:  $\beta = 3.9$ : results for the  $Z_q^{\text{pert}}$  ( $\mu = 10$  GeV) and  $c_{a2p2}$  Eq. (5.1) from the one-window hypercubic corrected data and the estimated  $g^2 \langle A^2 \rangle$  vev from the  $1/p^2$ , plotted as a function of the upper bound of the fitting range (in GeV).

prescription	$Z_q^{\text{pert}}$	$c_{a2p2}$	$g^2 \langle A^2 \rangle_{\text{tree}}$	$g^2 \langle A^2 \rangle_{CM}$
$\tilde{p}_\mu$	0.712(11)	-0.0026(23)	2.98(1.49)	2.53(1.23)
$p_\mu$	0.745(3)	-0.0061(8)	1.76(35)	1.45(29)

Table 6: For  $\beta = 3.9$ , results for the  $Z_q^{\text{pert}}(\mu^2, g_{\text{bare}}^2)$  ( $\mu = 10$  GeV) and  $c_{a2p2}$  Eq. (5.1) and  $g^2 \langle A^2 \rangle$  from the lattice data after a perturbative hypercubic correction.  $g^2 \langle A^2 \rangle$  is estimated at tree level from the  $1/p^2$  contribution.

the non-perturbative hypercubic correction, in tables 3 and 4. The  $\tilde{p}_\mu$  prescription has too large errors to be conclusive but the  $p_\mu$  is five sigmas away from zero, very similar to the results in table 4. The value of  $Z_q^{\text{pert}}$  for the  $\tilde{p}_\mu$  prescription is rather low but compatible within less than two sigmas from the result for  $\beta = 3.9$  in table 4.

### 5.3 Running of $Z_q^{\text{pert}}$

It is interesting to consider the dependence of  $Z_q^{\text{pert}}$  as a function of  $g^2$ . This is plotted in fig. 6 both for the OWF and the SWF. It is strikingly linear, specially for the OWF. Indeed from [26], eq. (24) perturbation theory gives a linear dependence with a slope  $\simeq -0.19$ . This comes from the coefficient  $b_{q1}$  in Eq. (4.1) which is multiplied by  $g^2$ . In our case we find from the OWF

$$\begin{aligned}
Z_q^{\text{pert}}((10 \text{ GeV})^2, g_{\text{bare}}^2) &= 0.737(3) - 0.313(6) (g_{\text{bare}}^2 - 1.5) , \\
Z_q^{\text{pert}}((2 \text{ GeV})^2, g_{\text{bare}}^2) &= 0.766(3) - 0.324(6) (g_{\text{bare}}^2 - 1.5) ;
\end{aligned} \tag{5.6}$$

and from the SWF

$$\begin{aligned}
Z_q^{\text{pert}}((10 \text{ GeV})^2, g_{\text{bare}}^2) &= 0.751(2)(7) - 0.273(6) \binom{0.002}{-0.038} (g_{\text{bare}}^2 - 1.5) , \\
Z_q^{\text{pert}}((2 \text{ GeV})^2, g_{\text{bare}}^2) &= 0.780(3)(7) - 0.284(6) \binom{0.002}{-0.040} (g_{\text{bare}}^2 - 1.5) .
\end{aligned} \tag{5.7}$$

We see that the coefficients of  $g^2$ ,

$$\frac{\partial Z_q^{\text{pert}}((2 \text{ GeV})^2, g_{\text{bare}}^2)}{\partial g^2} = \begin{cases} -0.329(6) & \text{OWF} \\ -0.287(26) & \text{SWF} \end{cases} , \tag{5.8}$$

are significantly larger than the perturbatively expected,  $-0.19$ . But the linear behaviour predicted by perturbation theory is well verified, especially for OWF.

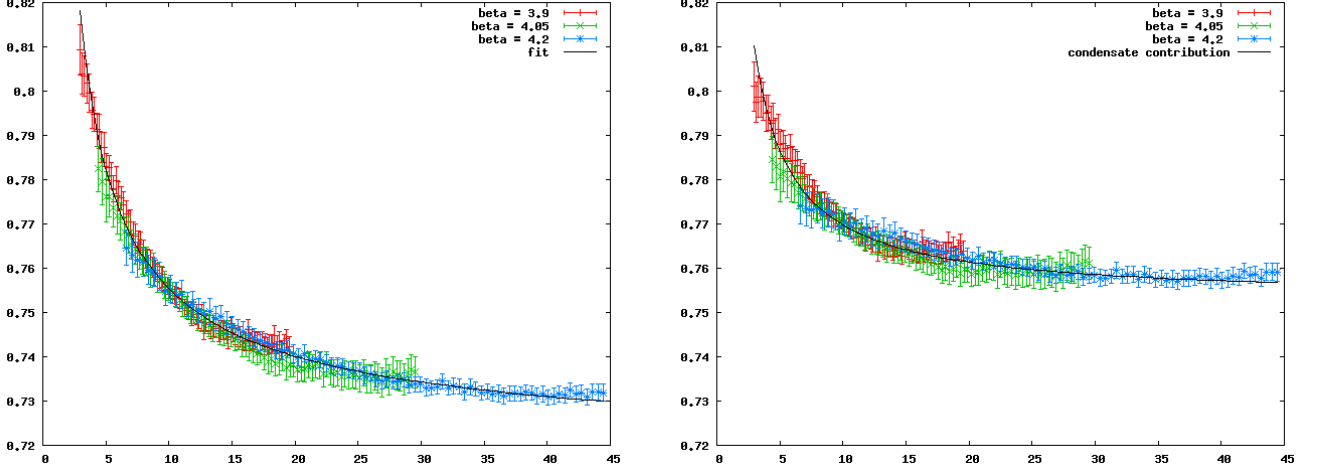


Figure 8: The merged plot with the OWF results at  $\beta = 4.05$  and  $\beta = 4.2$  rescaled to the  $\beta = 3.9$  thanks to the ratios of  $Z_q^{\text{pert}}$  given in table 3. The l.h.s shows the data corrected for all lattice artefacts. The r.h.s shows the same data furthermore corrected by the perturbative running factor up to 10 GeV. The horizontal axis is  $p^2$  in  $\text{GeV}^2$ . The black line on the l.h.s corresponds to the global fit with perturbative running and CM (three loops) wilson coefficient for the  $1/p^2$  term. The black line on the r.h.s corresponds only to the  $1/p^2$  times the three loops wilson coefficient added to  $Z_q^{\text{pert}}((10 \text{ GeV})^2, 6/3.9) = 0.726$

## 5.4 Merging the three lattice spacings.

From Eq. (5.1) and Eq. (5.5) it is clear that

$$Z_q^{\text{RI}'}(p^2, g_{\text{bare}}^2) = Z_q^{\text{hyp-corrected}}(a^2 p^2) - c_{a2p2} a^2 p^2. \quad (5.9)$$

In this section we use the one window fit, section 3.3.2, and the momentum  $p^2$  is now expressed in physical units. For the coefficient  $c_{a2p2}$  we use the values in table 3:  $c_{a2p2} = 0.0174$ . The three  $Z_q^{\text{RI}'}$  for the three  $\beta$ 's do not match due to the running of  $Z_q$  as a function of the lattice spacing. To make them match it turns out that it is enough to take into account the ratios of  $Z_q^{\text{pert}}$ 's given in table 3. We plot on the l.h.s of fig. 8 the three sets of data where the  $\beta = 4.05, 4.2$  ones have been rescaled to the  $\beta = 3.9$  scale. We see a rather good overlap. There is however a flattening at the right end of every  $\beta$  which stays within one sigma from the other  $\beta$ 's. We understand it as a failure of the hypercubic artefacts treatment. On the r.h.s side of fig. 8 we plot the same number corrected for perturbative running by the multiplicative factor  $0.726/Z_q^{\text{pert}}(p^2, 6/3.9)$ , where 0.726 is taken from table 7. The black line is just the non-perturbative contribution added to 0.726.



The comparison of both plots in Fig. 8 is enlightening. We see that the non perturbative term contributes about one half of the change between the smallest momenta and the largest ones. Both the perturbative running and the non perturbative contribution are convex, which makes it difficult to disentangle them. But we also see that the perturbative running cannot account for the full variation of the data. The best-fit parameters resulting from this merged analysis can be found in table 7, where we use  $g_{\text{bare}}^2 = 6.0/3.9$  since we have rescaled all the data to the  $\beta = 3.9$  one. The values in table 7 for  $g^2(\mu^2)\langle A^2 \rangle_{\mu^2 \text{ merged}}$  turn out to be rather central in the set of values of tables 3 and 4. The value for  $Z_q^{\text{pert}}(10 \text{ GeV}, 6./3.9)$  is in very good agreement with Eq. (5.6):  $Z_q^{\text{pert}}(10 \text{ GeV}, 6./3.9) = 0.725(3)$ .

$Z_q^{\text{pert}}$	$g^2\langle A^2 \rangle_{\text{tree}}$	$g^2\langle A^2 \rangle_{\text{CM}}$
0.726(2)	3.13(43)	2.55(36)

Table 7: Merged data from three  $\beta$ 's: results for the  $Z_q^{\text{pert}}$  ( $\mu = 10 \text{ GeV}$ ) rescaled to  $\beta = 3.9$ , from the one-window hypercubic corrected data (OWF) with tree level and the three loop formula, Eq. (A.24).

## 5.5 Summarizing

Many of our results for  $g^2\langle A^2 \rangle$  are shown in the l.h.s of Fig. 5. We did not plot the range dependent data to not overload the plot but they fall in the range covered by the data plotted in Fig. 5. To summarise our results and estimate the systematic uncertainty we consider the set of values in tables 3, 4,5 and 7. We will make a separate average for the tree level data and the  $O(\alpha^4)$  (CM) ones since the comparison with estimates from other quantities, such as the coupling constant, need to be performed in the same scheme, expansion, order and scale. The scheme is  $\overline{\text{MS}}$  and the precise implementation is detailed in the appendix. We computed an average of all above-listed data, weighted by their inverse squared error. The inverse squared statistical error is the sum of the inverse squared errors. The systematic error is taken such as to incorporate the central values within the error-bars. This is rather conservative. For  $Z_q^{\text{pert}}$  we average Eq. (5.6) and Eq. (5.7) with a similar method. We get:

$$\begin{aligned}
g^2(\mu^2)\langle A^2 \rangle_{\mu^2 \text{ tree}} &= 2.45(14) \begin{pmatrix} +0.78 \\ -0.87 \end{pmatrix} \text{ GeV}^2 \quad \mu = 10 \text{ GeV} , \\
g^2(\mu^2)\langle A^2 \rangle_{\mu^2 \text{ CM}} &= 2.01(11) \begin{pmatrix} +0.61 \\ -0.73 \end{pmatrix} \text{ GeV}^2 \quad \mu = 10 \text{ GeV} , \\
Z_q^{\text{pert}}((10 \text{ GeV})^2, g_{\text{bare}}^2) &= 0.744(2)(7) - 0.311(6) \begin{pmatrix} +0.002 \\ -0.038 \end{pmatrix} (g_{\text{bare}}^2 - 1.5) , \\
Z_q^{\text{pert}}((2 \text{ GeV})^2, g_{\text{bare}}^2) &= 0.773(3)(7) - 0.323(6) \begin{pmatrix} +0.002 \\ -0.040 \end{pmatrix} (g_{\text{bare}}^2 - 1.5) ; \quad (5.10)
\end{aligned}$$

where the first error is statistical and the second the systematic one. The values of  $Z_q^{\text{RI}'}(p^2, g_{\text{bare}}^2)$  may then be derived from Eq. (5.5):

$$Z_q^{\text{RI}'}((2 \text{ GeV})^2, g_{\text{bare}}^2) = 0.805(14) - 0.336(6) \begin{pmatrix} +0.002 \\ -0.042 \end{pmatrix} (g_{\text{bare}}^2 - 1.5) . \quad [\text{CM}] \quad (5.11)$$

The results obtained from the perturbative hypercubic correction, table 6 have not been used in the final estimate (because we did not compute them for all  $\beta's$ ) but they fall within the bounds at less than one sigma.

Finally two lines in the l.h.s. plot of fig. 5 show the results for  $g^2\langle A^2\rangle$  obtained from those in tab. 3 of ref. [7]:

$$g^2\langle A^2\rangle_{10\text{ GeV}} = \begin{cases} 4.1 \pm 1.5 \text{ GeV}^2 & \text{leading log} \\ 2.5 \pm 0.9 \text{ GeV}^2 & \mathcal{O}(\alpha^4) \end{cases} . \quad (5.12)$$

These values in Eq. (5.12) come from a totally different quantity: they have been extracted from the running of the ghost-gluon coupling constant. The results of ref. [7] were obtained by applying an OPE formula including a Wilson coefficient approximated at the leading logarithm and at the order  $\mathcal{O}(\alpha^4)$ , but expanded in terms of  $\alpha_T$ . Then, in order to be properly compared with the results of this work, the values of Eq. (5.12) incorporate the correction by the effect of expanding the OPE formula in terms of the running coupling in  $\overline{\text{MS}}$ . The lattice spacing applied in ref. [7] to get a physical scale,  $a(3.9) = 0.0801$  fm, was also slightly smaller than the one used in this work (see, for instance, tab. 1) and this has been also taken into account in obtaining Eq. (5.12).

As a matter of fact, Eq. (5.12) exhibits a slower convergence of the perturbative series of the Wilson-coefficient as in the present paper. From tables 3, 4, 5 and 7 we see that the  $\mathcal{O}(\alpha^4)$  estimate is about 20 % below the tree level while in table 3 of [7] it is about 45 % below the leading logarithm one. The two estimates agree rather well within the present accuracy.

## 5.6 Conversion to $\overline{\text{MS}}$

The conversion to  $\overline{\text{MS}}$  can also be performed from  $Z_q^{\text{pert}}$  or  $Z_q^{\text{RI}'}$  which contains a non-perturbative contribution. Usually, in the literature, the values are assumed to be perturbative. The conversion of  $Z_q^{\text{pert}}$  into  $\overline{\text{MS}}$  will use the standard perturbative conversion formulae [13]. We get

$$\begin{aligned} Z_q^{\overline{\text{MS}}\text{pert}}((2\text{ GeV})^2, g_{\text{bare}}^2) / Z_q^{\text{pert}}((2\text{ GeV})^2, g_{\text{bare}}^2) &= 0.97 , \\ Z_q^{\overline{\text{MS}}\text{pert}}((2\text{ GeV})^2, g_{\text{bare}}^2) &= 0.750(3)(7) - 0.313(20)(g_{\text{bare}}^2 - 1.5) . \end{aligned} \quad (5.13)$$

The central value of this result is about a 2 % systematically below the results of [28]. This can be presumably interpreted as a small systematic correction due to our subtraction of the non-perturbative contribution in obtaining  $Z_q^{\text{pert}}$  in the RI'-MOM scheme and converting it to  $Z_q^{\overline{\text{MS}}\text{pert}}$  at 2 GeV.

From Eq. (A.24) it is easy to see how to include the  $g^2\langle A^2\rangle$  non perturbative contribution. Up to now we have applied the result of the appendix using RI'-MOM for the perturbative part and  $\overline{\text{MS}}$  for the ratio in the corrective parenthesis. Had we wished to use the  $\overline{\text{MS}}$  scheme for the perturbative contribution, we would have the main inconvenience of not to know the OPE contribution for  $Z_q$  defined in the  $\overline{\text{MS}}$  scheme. However, only in the aim of roughly estimating the

non-perturbative correction, we can assume the OPE corrective parenthesis to remain the same and then get

$$Z_q^{\overline{\text{MS}}\text{non-perturbative}}((2\text{ GeV})^2, g_{\text{bare}}^2) = 0.781(6)(21) - 0.326(21) (g_{\text{bare}}^2 - 1.5) . \quad (5.14)$$

Notice that the non perturbative contribution is about 4% at 2 GeV. Nevertheless, the results of [28] have been obtained at momenta larger than 2 GeV. Although their estimates and our  $Z_q^{\text{RI}'}$  may agree with each other, a subtraction of the non-perturbative contribution in obtaining  $Z_q^{\text{pert}}$ , probably still required at the fitting window of [28] but not applied, could explain the small discrepancy of about a 2 % that we discussed above. The discrepancy is anyhow only affecting the conversion of  $Z_q^{\text{RI}'}$  to  $Z_q^{\overline{\text{MS}}\text{pert}}$  at 2 GeV. In Table 6 of [28] one finds results for  $Z_q^{\overline{\text{MS}}}$  obtained at 2 GeV by applying the standard perturbative conversion formulae [13]. Indeed, they turn out to be in between our results in Eq. (5.13) and Eq. (5.14). Quoting in order Eq. (5.13), ref. [28] and Eq. (5.14) we get: 0.738, 0.751 and 0.769 for  $\beta = 3.9$  and 0.755, 0.780 and 0.786 for  $\beta = 4.05$ .

## 5.7 Comparison of different estimates for the gluon condensate

Let us now compare the present estimate of  $g^2\langle A^2 \rangle$  to previous ones at  $N_f = 2$  and  $N_f = 0$ , all taken at the renormalisation scale of 10 GeV and, when needed, transformed to the very precise renormalization scheme for the OPE expansion defined in the appendix A.

In [4] a quenched study of  $Z_q$  using Wilson-Clover and overlap fermions ended with values of  $\langle A^2 \rangle_{\text{MOM}}$  in the range 2.67-3.2 GeV<sup>2</sup> with typical errors of 0.3 GeV<sup>2</sup>. Notice that this computation was performed only up to leading logarithm for the Wilson coefficient and that the choice was to expand the perturbative series in terms of the coupling renormalized in the MOM scheme (this is why we use for the VEV the label MOM). Then, we can apply the expressions derived in the appendix A to obtain the estimates for  $g^2\langle A^2 \rangle$  in the above-mentioned renormalization scheme appearing in table 8. However it is advocated in [4] that the  $1/p^2$  contribution only increases by 10% when going from MOM to  $\overline{\text{MS}}$ . On the other hand we have seen that between tree level and three loops a decrease of 20% was observed. In [4] an artefact  $\propto a/p^2$  was observed. We do not see it in the present analysis since the scaling of  $g^2\langle A^2 \rangle$  as a function of the lattice spacing indicates no visible  $1/p^2$  contribution dependent on  $a$ .

In [6] a summary was performed of different estimates of  $g^2\langle A^2 \rangle$  from gluonic quantities at  $N_f = 0$  :  $\alpha_s$  from the three gluon vertex with equal momenta on the three legs (symmetric) and from the three gluon vertex with one vanishing momentum (asymmetric), the ratio between the ghost and gluon propagators and  $\alpha_s$  from the ghost and gluon propagators, using Taylor's theorem. The ones involving gluon and ghost propagators agree fairly well but the latter is the most accurate. It gives  $g_T^2\langle A^2 \rangle = 5.1_{-1.1}^{+0.7}$ , although the applied OPE formula was obtained by expanding the involved perturbative series in terms of  $\alpha_T$ . After the appropriate transformation, one obtains the result shown in table 8. We also quote in the table the estimate of  $g^2\langle A^2 \rangle$  from the symmetric three gluon vertex, more precise than the one coming from the asymmetric vertex, and that appeared to be much higher than the estimate from  $\alpha_T$  and compatible with that from

quark propagator. In the case of the three-gluon estimates, no available  $O(\alpha^4)$  Wilson coefficient can help us to go beyond the leading logarithm approximation. However, either comparing the leading-logarithm estimates of the ones approximated at the order  $O(\alpha^4)$ , a clear discrepancy (by a factor of about two) appears between the estimates from ghost and gluon propagators and those from vertices or the quark propagator. This could imply that some systematic uncertainty is not completely under control. One might, for instance, guess that  $1/p^4$ -contributions can be invoked to reduce that discrepancy. For this to happen, the  $1/p^4$ -contributions had to be negative, and to tend to increase the estimate of  $g^2\langle A^2 \rangle$ , for the OPE formula of  $\alpha_T$ ; while it had to be positive, and reduce  $g^2\langle A^2 \rangle$ , for the quark propagator. Indeed, although no stable fit including  $1/p^4$ -contributions can be performed, the sign seems to be the right one for  $\alpha_T$  in [7]. Also the right sign of the contributions to  $Z_q$  is found in ref. [4].

measurement (GeV <sup>2</sup> )				
$N_f$	order $g^2\langle A^2 \rangle$	$Z_q$	$\alpha_T$	3-gluon
0	LL	9.4(3)	5.2(1.1)	10(3)
	$O(\alpha^4)$	9.0(3)	3.7(8)	
2	LL	2.7(4)	4.1(1.5)	
	$O(\alpha^4)$	2.55(36)	2.5(9)	

Table 8: Comparison of estimates of  $g^2\langle A^2 \rangle$  from different quantities an  $N_f = 0$  and  $N_f = 2$ . All are taken at the scale  $\mu = 10$  GeV. LL means leading logarithm for the Wilson coefficient.  $O(\alpha^4)$  refers to Chetyrkin and Maier computation.

In [7] the strong coupling constant was computed along similar lines to what is done here, on the same set of ETMC gauge configurations with  $N_f = 2$ . The necessity of a non-perturbative  $\propto 1/p^2$  contribution was also found and the resulting condensate,  $g^2\langle A^2 \rangle_{10 \text{ GeV}} = 2.3(8)$ , obtained through an OPE formula approximated at the  $O(\alpha^4)$ -order and expanded in  $\alpha_T$ , can be properly transformed<sup>5</sup> to give the value of table 8, also quoted in Eq. (5.12), which agrees strikingly well with the result of tab. 7 (the one we also quote in tab. 8) or that of Eq. (5.10). The value obtained through a leading-logarithm-approximated formula is also displayed in tab. 8. In [10] Martinelli and Sachrajda proposed a criterium to validate the use of operator expansion which we apply in this paper. They concluded that one should compare the difference of the highest order of the perturbative expansion for two different quantities with the non-perturbative contribution and check that the former is small compared to the latter. We have compared the highest order of the perturbative expansion of  $Z_q$  with the  $1/p^2$  contribution and find that the ratio ranges between 1/10 and 1/3 depending on the momentum. This is a good indication of the validity of our use of the operator expansion. Had we used the perturbative expansion only up to  $O(\alpha)$  the criterium would not have been fulfilled.

Furthermore, all these estimates in table 8 show a clear tendency of a decrease of  $g^2\langle A^2 \rangle$  from  $N_f = 0$  to  $N_f = 2$ . This might support an interpretation of  $g^2\langle A^2 \rangle$  as originating in instantons [30]

<sup>5</sup>We have taken into account the different lattice spacing in [7].

since the instanton density should decrease with light dynamical masses.

## 6 Conclusion

We have studied with care the twisted quark propagators produced on the ETMC set of  $N_f = 2$  gauge configurations. Our goal was to concentrate on two major issues: the correction for lattice spacing artefacts, particularly the hypercubic ones, and the presence of a sizeable non perturbative contribution of the  $A^2$  operator. The latter is expected to be sizeable because it was seen in the quenched case [4], it was seen in the unquenched study of the strong coupling constant [7] and since the Wilson coefficient of  $g^2\langle A^2 \rangle$  is not small in  $Z_q$  [9]. This is an important issue since from our estimates it gives a  $\sim 4\%$  contribution at 2 GeV. A reliable estimate of this non-perturbative correction needs a large enough fitting range, which allows to distinguish a  $1/p^2$  contribution from perturbative logarithms. But the fitting window is restricted below by infrared effects and above by lattice spacing artefacts. We thus need to improve our control on dominant lattice spacing artefacts which are of two types: hypercubic ones and  $\propto a^2 p^2$  ones.

Concerning the hypercubic artefacts, we have summarized the non-perturbative correcting method [24, 25] which we compared systematically with the perturbative results of [26].  $Z_q$  has very large hypercubic artefacts which display, as a function of  $p^2$  a “half-fishbone” very far from a smooth curve (see Fig. 1). We check carefully how these fishbones are “swallowed” by the corrective methods. It is worthwhile to emphasize that the “democratic” method, prescribing for instance a cut on  $p^{[4]}/p^2$  to drastically reduce the number of allowed hypercubic orbits, is not good enough to eliminate the fishbones and to leave us with a smooth curve for  $Z_q$ .

The perturbative method to correct hypercubic artefacts suffers from some options left: what to take for the coupling constant, use of  $p_\mu$  or  $\tilde{p}_\mu = a^{-1} \sin(ap_\mu)$ ? We tried first to stick to the prescription of [26] and use the boosted coupling constant. This reduces the hypercubic artefacts only up to  $a^2 p^2 \simeq 1.6$  (see Fig. 2, l.h.s). Guided by the test on the fishbone reduction we then propose a prescription based on the same perturbative formulae but using  $p_\mu$ . For  $Z_q$  this reduces the hypercubic artefacts up to  $a^2 p^2 \simeq 3.5$  which has been our upper bound in this work (see Fig. 2, r.h.s).

We test also the non-perturbative method to correct hypercubic artefacts. We use two prescriptions. The first one uses a sliding window and the second one uses only one fitting window on the full momentum range.

We find that the hypercubic artefacts are sufficiently well described and cured by two terms:  $\propto a^2 p^{[4]}/p^2$  and  $\propto a^4 p^{[4]}$ . We fit the coefficients of these quantities and check their scaling with  $\beta$ .

From the resulting hypercubic corrected function  $Z_q(a^2 p^2, a^2 \Lambda_{\text{QCD}}^2)$  we perform fits which incorporate the perturbative running, a non perturbative  $1/p^2$  term (presumably related to  $g^2\langle A^2 \rangle$ ), and a hypercubic insensitive lattice spacing artefact proportional to  $a^2 p^2$ . The fits are good. The  $a^2 p^2$  term scales almost perfectly in lattice units, as expected. The  $g^2\langle A^2 \rangle$  term scales rather well in physical units as expected. The accuracy on  $g^2\langle A^2 \rangle$  is reduced by some correlations in the fits: we see a correlation between the method used to correct hypercubic artefacts and the estimated

value of  $g^2\langle A^2 \rangle$ . We also see a correlation between the fitting range and the resulting  $g^2\langle A^2 \rangle$ . But all values of  $g^2\langle A^2 \rangle$  fall into the same ballpark and none of these fits can be done without such a positive contribution. To estimate the systematic uncertainty we have considered a large panel of fitting methods. All at more than four sigmas from zero except at  $\beta = 4.2$  with the sliding window where they are only 2.5 sigmas above zero. Comparing the fitted  $\langle A^2 \rangle$  using the tree level Wilson coefficient and that using the three loops one, we find that the latter is about 20 % below the former.

The perturbative contribution to  $Z_q$ ,  $Z_q^{\text{pert}}$  has a linear dependence in the bare lattice coupling: see Fig. 6 and Eq. (5.10), as expected from perturbation theory, but with a larger coefficient, even when the boosted coupling constant is used in perturbation theory.

We also merge all three  $\beta$ 's after having subtracted the  $a^2 p^2$  term and rescaled the  $\beta = 4.05, 4.2$  to 3.9 using the ratios of  $Z_q^{\text{pert}}(\mu)$ . The overlap of the three data sets is rather good. The need of a non-perturbative contribution is also visible there. Both perturbative and non-perturbative contributions decrease with the momentum and are convex. This makes the separation difficult. Grossly speaking they share the decrease between 4 and 40 GeV<sup>2</sup> in equal parts.

We have converted our results for  $Z_q^{\text{RI}'}$  and its perturbative part  $Z_q^{\text{pert}}(\mu)$  into the  $\overline{\text{MS}}$  scheme. Combining all the results we find, using the three loop Wilson coefficient:

$$\begin{aligned}
g^2(\mu^2)\langle A^2 \rangle_{\mu^2 \text{ CM}} &= 2.01(11) \left( \begin{smallmatrix} +0.61 \\ -0.73 \end{smallmatrix} \right) \text{ GeV}^2 \quad \mu = 10 \text{ GeV} , \\
Z_q^{\text{pert}}((2 \text{ GeV})^2, g_{\text{bare}}^2) &= 0.773(3)(7) - 0.323(6) \left( \begin{smallmatrix} +0.002 \\ -0.040 \end{smallmatrix} \right) (g_{\text{bare}}^2 - 1.5) , \\
Z_q^{\text{RI}'}((2 \text{ GeV})^2, g_{\text{bare}}^2) &= 0.805(14) - 0.323(6) \left( \begin{smallmatrix} +0.002 \\ -0.040 \end{smallmatrix} \right) (g_{\text{bare}}^2 - 1.5) , \\
Z_q^{\overline{\text{MS}} \text{ pert}}((2 \text{ GeV})^2, g_{\text{bare}}^2) &= 0.750(3)(7) - 0.313(20) (g_{\text{bare}}^2 - 1.5) , \\
Z_q^{\overline{\text{MS}} \text{ non-perturbative}}((2 \text{ GeV})^2, g_{\text{bare}}^2) &= 0.781(6)(21) - 0.313(20) (g_{\text{bare}}^2 - 1.5) ; \quad (6.1)
\end{aligned}$$

where the systematic error is estimated from the scattering of the results in tables 3, 4, 5 and 7. We use the lattice spacings listed in table 1.

Futhermore, table 8 also shows a nice agreement between the condensates for  $N_f = 2$ , although some systematics appears not to be under control for  $N_f = 0$ . This supports the interpretation of the  $\propto 1/p^2$  contribution as being due to a condensate of the only dimension two operator in Landau gauge:  $A^2$ . Another confirmation comes from the validity of Martinelli-Sachrajda's criterium [10]. The accuracy on  $g^2\langle A^2 \rangle$  is however limited due to several correlations in the fits. Further and more accurate checks of the consistency of  $g^2\langle A^2 \rangle$  from other renormalisation constants will be very welcome.

## Acknowledgements

We thank Alain Le Yaouanc, Vittorio Lubicz and Gian-Carlo Rossi for a critical reading of this manuscript and the very useful subsequent discussions. This work was granted access to the HPC resources of CINES and IDRIS under the allocation 2010-052271 made by GENCI. J. R-Q is

indebted to the Spanish MICINN for the support by the research project FPA2009-10773 and to “Junta de Andalucía” by P07FQM02962. Z. Liu thanks the UK Science and Technology Facilities Council (STFC) for financial support.

## A Appendix: The Wilson coefficients at $O(\alpha^4)$

The purpose of this appendix is to describe briefly the OPE analysis of the quark propagator renormalization constant defined in Eq. (1.2) that leads us to Eq. (5.1), where the four-loops results in ref. [9] are exploited to derive the Wilson coefficients with the appropriate renormalization prescription. This OPE analysis is analogous to the one performed in refs. [2, 3, 5, 6]. The starting point is the OPE of the inverse of the quark propagator:

$$\begin{aligned} S^{-1}(p^2, \mu^2) &= Z_q^{-1}(\mu^2) S_{\text{bare}}^{-1}(p^2) = (S^{\text{pert}})^{-1}(p^2, \mu^2) + i\not{p} \frac{c_{2Z_q}\left(\frac{p^2}{\mu^2}, \alpha(\mu)\right)}{p^2} \frac{\langle A^2 \rangle_{R, \mu^2}}{4(N_c^2 - 1)} \delta_{ab} \\ &= \frac{(S_{\text{bare}}^{\text{pert}})^{-1}(p^2)}{Z_q^{\text{pert}}(\mu^2)} + i\not{p} \frac{c_{2Z_q}\left(\frac{p^2}{\mu^2}, \alpha(\mu)\right)}{p^2} \frac{\langle A^2 \rangle_{R, \mu^2}}{4(N_c^2 - 1)} \delta_{ab} , \end{aligned} \quad (\text{A.1})$$

where only the leading term in  $\not{p}$  is kept, the quark mass being assumed to be negligible or to vanish. The cut-off regularization dependence is omitted for the bare quantities but that on the renormalization momentum,  $\mu$ , is explicitly written for the renormalized ones. In the RI'-MOM scheme we define  $Z_q^{\text{RI}'}$  such that  $(S_{\text{bare}})^{-1}(p^2) = i\not{p} \delta_{ab} Z_q^{\text{RI}'}(p^2)$  and  $Z_q^{\text{pert RI}'}$  such that,  $(S_{\text{bare}}^{\text{pert}})^{-1}(p^2) = i\not{p} \delta_{ab} Z_q^{\text{pert RI}'}(p^2)$ . Then, the renormalization momentum,  $\mu^2$ , taken to lie on the perturbative regime, one can apply Eq. (1.2) and obtain,

$$\begin{aligned} \frac{Z_q^{\text{RI}'}(p^2)}{Z_q^{\text{pert}}(\mu^2)} &= \frac{Z_q^{\text{pert RI}'}(p^2)}{Z_q^{\text{pert}}(\mu^2)} + c_{2Z_q}\left(\frac{p^2}{\mu^2}, \alpha(\mu)\right) \frac{\langle A^2 \rangle_{R, \mu^2}}{4(N_c^2 - 1)p^2} \\ &= c_{0Z_q}\left(\frac{p^2}{\mu^2}, \alpha(\mu)\right) + c_{2Z_q}\left(\frac{p^2}{\mu^2}, \alpha(\mu)\right) \frac{\langle A^2 \rangle_{R, \mu^2}}{4(N_c^2 - 1)p^2} . \end{aligned} \quad (\text{A.2})$$

which implies a definition of  $c_{0Z_q}$  and where  $c_{2Z_q}(p^2, \mu^2)$  is the Wilson coefficient of  $g^2 \langle A^2 \rangle$ . Although not yet specifying the renormalisation scheme of  $Z_q^{\text{pert}}(\mu^2)$ , we know that

$$c_{0Z_q}(1, \alpha(\mu)) = 1 + O(\alpha^2) , \quad (\text{A.3})$$

while  $c_{2Z_q}$  is known up to  $O(\alpha^4)$  in the  $\overline{\text{MS}}$  scheme [9] and, in particular,  $c_{2Z_q}^{\overline{\text{MS}}}(1, \alpha(\mu))$  is given in eq (18) of that paper using  $q^2 = \mu^2$ . Let us however keep in mind that

$$c_{2Z_q}(1, \alpha(\mu)) = \frac{32\pi}{3} \alpha(\mu) (1 + \mathcal{O}(\alpha(\mu))) = \frac{8g^2(\mu)}{3} (1 + \mathcal{O}(\alpha(\mu))) . \quad (\text{A.4})$$

Now, with the help of the appropriate renormalization constants, one can also write Eq. (A.2) in terms of bare quantities:

$$\begin{aligned} Z_q^{\text{RI}'}(p^2) &= Z_q^{\text{pert}}(\mu^2) c_{0Z_q} \left( \frac{p^2}{\mu^2}, \alpha(\mu) \right) \\ &+ Z_q^{\text{pert}}(\mu^2) Z_{A^2}^{-1}(\mu^2, \Lambda^2) c_{2Z_q} \left( \frac{p^2}{\mu^2}, \alpha(\mu) \right) \frac{\langle A^2 \rangle}{4(N_c^2 - 1)p^2}, \end{aligned} \quad (\text{A.5})$$

where  $A_R^2 = Z_{A^2}^{-1} A^2$ . Then, as the  $\mu$ -dependence of both l.h.s. and r.h.s. of Eq. (A.5) should match each other for any  $p$ , one can take the logarithmic derivative with respect to  $\mu$  and infinite cut-off limit, term by term, on r.h.s. and obtains:

$$\begin{aligned} \gamma_q(\alpha(\mu)) + \left\{ \frac{\partial}{\partial \log \mu^2} + \beta(\alpha(\mu)) \frac{\partial}{\partial \alpha} \right\} \ln c_{0Z_q} \left( \frac{q^2}{\mu^2}, \alpha(\mu) \right) &= 0 \\ -\gamma_{A^2}(\alpha(\mu)) + \gamma_q(\alpha(\mu)) + \left\{ \frac{\partial}{\partial \log \mu^2} + \beta(\alpha(\mu)) \frac{\partial}{\partial \alpha} \right\} \ln c_{2Z_q} \left( \frac{q^2}{\mu^2}, \alpha(\mu) \right) &= 0, \end{aligned} \quad (\text{A.6})$$

where the  $\beta$ -function, chosen to be in  $\overline{\text{MS}}$ , is defined as

$$\beta(\alpha(\mu)) = \frac{d}{d \log \mu^2} \alpha(\mu) = -4\pi \sum_{i=0} \beta_i \left( \frac{\alpha(\mu)}{4\pi} \right)^{i+2} \quad (\text{A.7})$$

and where  $\gamma_q(\alpha(\mu))$  and  $\gamma_{A^2}(\alpha(\mu))$  are the anomalous dimensions for the fermion propagator and local operator  $A^2$ , respectively, which are formally defined as

$$\gamma_X(\alpha(\mu)) = \frac{d}{d \log \mu^2} \log Z_X = - \sum_{i=0} \gamma_i^X \left( \frac{\alpha(\mu)}{4\pi} \right)^{i+1}, \quad (\text{A.8})$$

where  $X$  stands for  $q$  or  $A^2$ . The scheme for the anomalous dimension of  $Z_{A^2}$  is imposed through the renormalization of the local operator  $A^2$ , as was done in ref. [2] to obtain its leading logarithm contribution, and it is only known in the  $\overline{\text{MS}}$  at the order  $\mathcal{O}(\alpha^4)$  [29]. Then, that is the only possible choice of scheme for  $\gamma_{A^2}$  in eqs. (A.6). Concerning  $Z_q^{\text{pert}}$ , its scheme is determined by the renormalization prescription for the non-perturbative propagator in the left hand-side of Eq. (A.1). Both  $\overline{\text{MS}}$  and RI'-MOM are possible. As we aim to obtain a non-perturbative formula to be confronted to the lattice estimate of the RI'-MOM quark renormalization constant, it is convenient also to prescribe the RI'-MOM scheme for  $Z_q^{\text{pert}}$ . Thus, eqs. (A.6) must be re-written as

$$\begin{aligned} \gamma_q^{\text{RI}'}(\alpha(\mu)) + \left\{ \frac{\partial}{\partial \log \mu^2} + \beta(\alpha(\mu)) \frac{\partial}{\partial \alpha} \right\} \ln c_{0Z_q}^{\text{RI}'} \left( \frac{q^2}{\mu^2}, \alpha(\mu) \right) &= 0 \\ -\gamma_{A^2}^{\overline{\text{MS}}}(\alpha(\mu)) + \gamma_q^{\text{RI}'}(\alpha(\mu)) + \left\{ \frac{\partial}{\partial \log \mu^2} + \beta(\alpha(\mu)) \frac{\partial}{\partial \alpha} \right\} \ln c_{2Z_q}^{\text{WM}\overline{\text{MS}}} \left( \frac{q^2}{\mu^2}, \alpha(\mu) \right) &= 0, \end{aligned} \quad (\text{A.9})$$



where

$$c_{0Z_q}^{\text{RI}'} \left( \frac{p^2}{\mu^2}, \alpha(\mu) \right) \equiv \frac{Z_q^{\text{pert RI}'}(p^2)}{Z_q^{\text{pert RI}'}(\mu^2)} \quad (\text{A.10})$$

and  $c_{2Z_q}^{\overline{\text{WMS}}}$  is in the  $\overline{\text{WMS}}$  scheme<sup>6</sup> explicitly defined by the second equation of (A.9), after the RI'-MOM prescription for  $Z_q^{\text{pert}}$ , that of  $\overline{\text{MS}}$  for  $A^2$  and by the choice of a boundary condition,  $c_{2Z_q}^{\overline{\text{WMS}}}(1, \alpha(q))$ . Then, from Eq. (A.2) one obtains

$$Z_q^{\text{RI}'}(p^2) = Z_q^{\text{pert RI}'(\mu^2)} c_{0Z_q}^{\text{RI}'} \left( \frac{p^2}{\mu^2}, \alpha(\mu) \right) \left( 1 + \frac{c_{2Z_q}^{\overline{\text{WMS}}} \left( \frac{p^2}{\mu^2}, \alpha(\mu) \right)}{c_{0Z_q}^{\text{RI}'} \left( \frac{p^2}{\mu^2}, \alpha(\mu) \right)} \frac{\langle A^2 \rangle_{R, \mu^2}}{4(N_c^2 - 1)p^2} \right), \quad (\text{A.11})$$

and, in practice, both eqs. (A.9) can be combined to give the following differential equation,

$$\left\{ -\gamma_{A^2}^{\overline{\text{MS}}}(\alpha(\mu)) + \frac{\partial}{\partial \log \mu^2} + \beta(\alpha(\mu)) \frac{\partial}{\partial \alpha} \right\} \frac{c_{2Z_q}^{\overline{\text{WMS}}} \left( \frac{p^2}{\mu^2}, \alpha(\mu) \right)}{c_{0Z_q}^{\text{RI}'} \left( \frac{p^2}{\mu^2}, \alpha(\mu) \right)} = 0, \quad (\text{A.12})$$

that can be solved to provide us with the ratio of Wilson coefficients,  $c_{2Z_q}/c_{0Z_q}$ , required to implement Eq. (A.11). For the purpose of the best comparison with the results from the analysis performed in ref. [6], we applied

$$c_{2Z_q}^{\overline{\text{WMS}}}(1, \alpha(p)) \equiv c_{2Z_q}^{\overline{\text{MS}}}(1, \alpha(p)), \quad (\text{A.13})$$

where  $c_{2Z_q}^{\overline{\text{MS}}}(1, \alpha(\mu))$  is taken from eq. (18) of ref. [9] using  $q^2 = \mu^2$ , as a boundary condition which is equivalent to the one applied in the analysis of ref. [6].

On the other hand, if we take  $Z_q^{\text{pert}}$  to be renormalized in  $\overline{\text{MS}}$ , the equations in (A.6) reads

$$\begin{aligned} \gamma_q^{\overline{\text{MS}}}(\alpha(\mu)) + \left\{ \frac{\partial}{\partial \log \mu^2} + \beta(\alpha(\mu)) \frac{\partial}{\partial \alpha} \right\} \ln c_{0Z_q}^{\overline{\text{MS}}} \left( \frac{q^2}{\mu^2}, \alpha(\mu) \right) &= 0 \\ -\gamma_{A^2}^{\overline{\text{MS}}}(\alpha(\mu)) + \gamma_q^{\overline{\text{MS}}}(\alpha(\mu)) + \left\{ \frac{\partial}{\partial \log \mu^2} + \beta(\alpha(\mu)) \frac{\partial}{\partial \alpha} \right\} \ln c_{2Z_q}^{\overline{\text{MS}}} \left( \frac{q^2}{\mu^2}, \alpha(\mu) \right) &= 0, \end{aligned} \quad (\text{A.14})$$

where  $c_{2Z_q}^{\overline{\text{MS}}}$  is the Wilson coefficient computed in ref. [9], provided that the boundary condition,  $c_{2Z_q}^{\overline{\text{MS}}}(1, \alpha(\mu))$ , is taken again from eq. (18) of the same paper using  $q^2 = \mu^2$ . Then, we can

---

<sup>6</sup>We define this scheme by imposing that the local operator of the Wilson expansion is renormalized in  $\overline{\text{MS}}$ , while the expanded operator (the quark propagator, in our case) is in a MOM scheme. We called this “Wilson  $\overline{\text{MS}}$ ”.

combine again Eqs. (A.14) to obtain for  $c_2^{\overline{\text{MS}}}/c_0^{\overline{\text{MS}}}$  the same equation Eq. (A.12) that, with the same boundary condition, leads to:

$$\frac{c_{2Z_q}^{\overline{\text{WMS}}}\left(\frac{p^2}{\mu^2}, \alpha(\mu)\right)}{c_{0Z_q}^{\text{RI}'}\left(\frac{p^2}{\mu^2}, \alpha(\mu)\right)} = \frac{c_{2Z_q}^{\overline{\text{MS}}}\left(\frac{p^2}{\mu^2}, \alpha(\mu)\right)}{c_{0Z_q}^{\overline{\text{MS}}}\left(\frac{p^2}{\mu^2}, \alpha(\mu)\right)}. \quad (\text{A.15})$$

On the other hand, we can also combine the second equation of (A.9) with the second one of Eq. (A.14) and obtain

$$\left\{ \gamma_q^{\text{RI}'}(\alpha(\mu)) - \gamma_q^{\overline{\text{MS}}}(\alpha(\mu)) + \frac{\partial}{\partial \log \mu^2} + \beta(\alpha(\mu)) \frac{\partial}{\partial \alpha} \right\} \frac{c_{2Z_q}^{\overline{\text{WMS}}}\left(\frac{p^2}{\mu^2}, \alpha(\mu)\right)}{c_{2Z_q}^{\overline{\text{MS}}}\left(\frac{p^2}{\mu^2}, \alpha(\mu)\right)} = 0, \quad (\text{A.16})$$

that, according to Eq. (A.13), can be solved with the boundary condition  $c_{2Z_q}^{\overline{\text{MS}}}(1, \alpha(p))/c_{2Z_q}^{\overline{\text{MS}}}(1, \alpha(p)) \equiv 1$  and leaves us with a relation of  $\overline{\text{WMS}}$  and  $\overline{\text{MS}}$  Wilson coefficients which allows Eq. (A.11) to be re-written as

$$\begin{aligned} Z_q^{\text{RI}'}(p^2) &= Z_q^{\text{pert RI}'}(\mu^2) c_{0Z_q}^{\text{RI}'}\left(\frac{p^2}{\mu^2}, \alpha(\mu)\right) \\ &\times \left( 1 + \frac{c_{2Z_q}^{\overline{\text{MS}}}\left(\frac{p^2}{\mu^2}, \alpha(\mu)\right)}{c_{0Z_q}^{\text{RI}'}\left(\frac{p^2}{\mu^2}, \alpha(\mu)\right)} \frac{c_{2Z_q}^{\overline{\text{WMS}}}\left(\frac{p^2}{\mu^2}, \alpha(\mu)\right)}{c_{2Z_q}^{\overline{\text{MS}}}\left(\frac{p^2}{\mu^2}, \alpha(\mu)\right)} \frac{\langle A^2 \rangle_{\overline{\text{MS}}, \mu^2}}{4(N_c^2 - 1)p^2} \right). \end{aligned} \quad (\text{A.17})$$

where, furthermore,  $c_{2Z_q}^{\overline{\text{MS}}}$  is to be taken from ref. [9] and  $c_{0Z_q}^{\text{RI}'}$  from ref. [13]. Thus, we can use either Eq. (A.11) with the solution of Eq. (A.9) or Eq. (A.17) with that of Eq. (A.16) to confront to the lattice estimates of  $Z_q^{\text{RI}'}$ . Both expressions are equivalent. In the first case, one can proceed as was done in ref. [7] to solve Eq. (A.9). To illustrate this first method, let us remind that Eq. (A.9) can be solved at the leading logarithm by applying the following ansatz,

$$\frac{c_{2Z_q}^{\overline{\text{WMS}}}\left(\frac{p^2}{\mu^2}, \alpha(\mu)\right)}{c_{0Z_q}^{\text{RI}'}\left(\frac{p^2}{\mu^2}, \alpha(\mu)\right)} = \frac{32\pi}{3} \alpha(p) \left( \frac{\alpha(\mu)}{\alpha(p)} \right)^a \left( 1 + \mathcal{O}(\alpha) \right), \quad (\text{A.18})$$

where we apply Eq. (A.4) and the exponent  $a$ , required to satisfy Eq. (A.9), should be

$$a = \frac{\gamma_0^{A^2}}{\beta_0} = \frac{105 - 8N_f}{132 - 8N_f}. \quad (\text{A.19})$$

In the second case, to solve Eq. (A.16), a similar ansatz extended to three-loops order can be applied,

$$\frac{c_{2Z_q}^{\overline{\text{MS}}} \left( \frac{p^2}{\mu^2}, \alpha(\mu) \right)}{c_{2Z_q}^{\overline{\text{MS}}} \left( \frac{p^2}{\mu^2}, \alpha(\mu) \right)} = \left( \frac{\alpha(\mu)}{\alpha(p)} \right)^b \left( \frac{1 + \sum_i r_i \left( \frac{\alpha(\mu)}{4\pi} \right)^i}{1 + \sum_i r_i \left( \frac{\alpha(p)}{4\pi} \right)^i} \right), \quad (\text{A.20})$$

where we use Eq. (A.13) for the boundary condition. Then, by requiring that the ansatz Eq. (A.20) verifies Eq. (A.16), the coefficients  $b$  and  $r_i$ 's will be obtained in terms of those for the fermion propagator  $\overline{\text{MS}}$  and RI'-MOM anomalous dimensions and for the  $\overline{\text{MS}}$   $\beta$ -function. However, in this case,

$$b = \frac{\gamma_0^{q\overline{\text{MS}}} - \gamma_0^{q\text{RI}'}}{\beta_0} = 0, \quad (\text{A.21})$$

because the first-loop coefficient for the anomalous dimension is scheme independent (in the particular Landau gauge, this scheme-independent first-loop coefficient is also zero for any scheme [13]). Furthermore, as can be seen in the appendix C of ref. [13], one is also left with  $\gamma_1^{q\overline{\text{MS}}} \equiv \gamma_1^{q\text{RI}'}$  in Landau gauge. Then,

$$r_1 = \frac{\gamma_1^{q\overline{\text{MS}}} - \gamma_1^{q\text{RI}'}}{\beta_0} = 0, \quad (\text{A.22})$$

and the Wilson coefficients for  $\overline{\text{MS}}$  and RI'-MOM will thus differ only at the order  $\mathcal{O}(\alpha^2)$ , with the non-zero  $r_i$ 's coefficients to be applied in Eq. (A.20) given by

$$\begin{aligned} r_2 &= \frac{\gamma_2^{q\overline{\text{MS}}} - \gamma_2^{q\text{RI}'}}{2\beta_0} = -25.4642 + 2.3333 N_f, \\ r_3 &= \frac{\gamma_3^{q\overline{\text{MS}}} - \gamma_3^{q\text{RI}'}}{3\beta_0} - \beta_1 \frac{\gamma_2^{q\overline{\text{MS}}} - \gamma_2^{q\text{RI}'}}{3\beta_0^2} = -1489.9796 + 246.4424 N_f - 6.4609 N_f^2; \end{aligned} \quad (\text{A.23})$$

where the three and four-loop coefficient in  $\overline{\text{MS}}$  and RI'-MOM for the fermion propagator anomalous dimension have been again obtained from ref. [13]. This leads, using Eqs. (A.17,A.20–A.23) with  $N_c^2 - 1 = 8$  and  $N_f = 2$ , to our final formulae for the free-of-artefacts lattice determination of  $Z_q$ :

$$\begin{aligned} Z_q^{\text{Latt artefree}}(p^2, \beta) &= Z_q^{\text{pert RI}'}(\mu'^2) c_{0Z_q}^{\text{RI}'} \left( \frac{p^2}{\mu'^2}, \alpha(\mu') \right) \\ &\times \left( 1 + \frac{c_{2Z_q}^{\overline{\text{MS}}} \left( \frac{p^2}{\mu^2}, \alpha(\mu) \right)}{c_{0Z_q}^{\text{RI}'} \left( \frac{p^2}{\mu^2}, \alpha(\mu) \right)} \frac{1 - 0.1317 \alpha^2(\mu) - 0.5155 \alpha^3(\mu)}{1 - 0.1317 \alpha^2(p) - 0.5155 \alpha^3(p)} \frac{\langle A^2 \rangle_{\overline{\text{MS}}, \mu^2}}{32 p^2} \right) \end{aligned} \quad (\text{A.24})$$

In this last equation, we exploited the fact that the expression in parenthesis in Eqs. (A.17,A.24) does not vary with the renormalization momentum for the local operator  $A^2$ , as can be inferred from Eq. (A.12). Thus, once a given momentum,  $\mu'^2$ , is fixed for the renormalization of the fermion propagator in the l.h.s. of Eq. (A.1), the one appearing in  $Z_q^{\text{pert RI}'}$  in front of the expression in parenthesis, one is still left with the freedom of choosing a renormalization momentum,  $\mu^2$ , which does not need to be the same, for the local operator  $A^2$  inside the parenthesis.

In Eq. (A.24) the coefficients  $c_{0Z_q}^{\text{RI}'}$  and  $c_{2Z_q}^{\overline{\text{MS}}}$  are known from perturbation theory, the former can be obtained from ref. [13] and the latter from ref. [9]. Two parameters are to be fitted:  $Z_q^{\text{pert RI}'}$  ( $\mu'^2$ ) and the non perturbative condensate  $g^2(\mu) \langle A^2 \rangle_{R,\mu^2}$ . It is important to underline that the condensate *is defined via the OPE, i.e. from Eqs. (A.17,A.24)*. Its precise definition depends on the renormalisation scheme, the renormalisation scale, as well as the order in perturbation theory to which the coefficients  $c_{0Z_q}$  and  $c_{2Z_q}$  are used. In Eq. (A.17) and Eq. (A.24) the renormalisation scheme for  $g^2(\mu) \langle A^2 \rangle_{R,\mu^2}$  is  $\overline{\text{MS}}$  and the scale is  $\mu$  (10 GeV in our calculations). The coupling we use for the perturbative expansions of these coefficients,  $c_{0Z_q}$  and  $c_{2Z_q}$ , is also chosen to be the  $\overline{\text{MS}}$  one. These choices are kept all along the present paper. If we now wish to compare  $g^2(\mu) \langle A^2 \rangle_{R,\mu^2}$  from the present calculation to that from another calculation, for example from the strong coupling constant [7], *we must as far as possible use the same precise definition in both cases*. However, its dependence on the scheme and on the order in perturbation theory is not so important: as seen in section 5 other systematic uncertainties are larger.

## References

- [1] M. Lavelle and M. Oleszczuk, *Mod. Phys. Lett. A* **7** (1992) 3617; J. Ahlback, M. Lavelle, M. Schaden and A. Streibl, *Phys. Lett. B* **275** (1992) 124.
- [2] P. Boucaud, A. Le Yaouanc, J. P. Leroy, J. Micheli, O. Pene and J. Rodriguez-Quintero, *Phys. Rev. D* **63** (2001) 114003 [arXiv:hep-ph/0101302];
- [3] P. Boucaud, A. Le Yaouanc, J. P. Leroy, J. Micheli, O. Pene and J. Rodriguez-Quintero, *Phys. Lett. B* **493** (2000) 315 [arXiv:hep-ph/0008043]; F. De Soto and J. Rodriguez-Quintero, *Phys. Rev. D* **63** (2001) 114003 [arXiv:hep-ph/0105063];
- [4] Ph. Boucaud *et al.*, *Phys. Rev. D* **74** (2006) 034505 [arXiv:hep-lat/0504017].
- [5] Ph. Boucaud *et al.*, *JHEP* **0601** (2006) 037 [arXiv:hep-lat/0507005];
- [6] Ph. Boucaud, F. De Soto, J. P. Leroy, A. Le Yaouanc, J. Micheli, O. Pene and J. Rodriguez-Quintero, *Phys. Rev. D* **79** (2009) 014508 [arXiv:0811.2059 [hep-ph]].
- [7] B. Blossier, Ph. Boucaud, F. De soto, V. Morenas, M. Gravina, O. Pene and J. Rodriguez-Quintero [ETM Collaboration], arXiv:1005.5290 [hep-lat].
- [8] E. Megias, E. Ruiz Arriola and L. L. Salcedo, *Phys. Rev. D* **75** (2007) 105019 [arXiv:hep-ph/0702055].
- [9] K. G. Chetyrkin and A. Maier, arXiv:0911.0594 [hep-ph].
- [10] G. Martinelli and C. T. Sachrajda, *Nucl. Phys. B* **478** (1996) 660 [arXiv:hep-ph/9605336].
- [11] F. V. Gubarev and V. I. Zakharov, *Phys. Lett. B* **501** (2001) 28 [arXiv:hep-ph/0010096]; K. G. Chetyrkin, S. Narison and V. I. Zakharov, *Nucl. Phys. B* **550** (1999) 353; D. Dudal, H. Verschelde and S. P. Sorella, *Phys. Lett. B* **555** (2003) 126; K. I. Kondo, *Phys. Lett. B* **572** (2003) 210; [arXiv:hep-th/0306195]. *Phys. Lett. B* **514** (2001) 335 [arXiv:hep-th/0105299];
- [12] P. Boucaud *et al.*, *Phys. Lett. B* **575** (2003) 256 [arXiv:hep-lat/0307026].
- [13] K. G. Chetyrkin and A. Retey, *Nucl. Phys. B* **583**, 3 (2000) [arXiv:hep-ph/9910332]; K. G. Chetyrkin, *Nucl. Phys. B* **710** (2005) 499 [arXiv:hep-ph/0405193]; <http://www-ttp.particle.uni-karlsruhe.de/Progdata/ttp99/ttp99-43/>
- [14] R. Wilson, *Phys. Rev.* **179** (1969) 1499.
- [15] M.A. Shifman, A.I. Vainshtein, V.I. Zakharov, *Nucl. Phys.* **B147** (1979) 385,447,519; M.A. Shifman, A.I. Vainshtein, M.B. Voloshin, V.I. Zakharov, *Phys. Lett.* **B77** (1978) 80;
- [16] P. Weisz, *Nucl. Phys. B* **212** (1983) 1.
- [17] R. Frezzotti, P. A. Grassi, S. Sint and P. Weisz [Alpha collaboration], *JHEP* **0108** (2001) 058 [arXiv:hep-lat/0101001].

- [18] Ph. Boucaud *et al.* [ETM collaboration], *Comput. Phys. Commun.* **179** (2008) 695 [arXiv:0803.0224 [hep-lat]].
- [19] Ph. Boucaud *et al.* [ETM Collaboration], *Phys. Lett. B* **650** (2007) 304 [arXiv:hep-lat/0701012].
- [20] C. Urbach [ETM Coll.], *PoS LAT2007* (2007) 022 [0710.1517 [hep-lat]].
- [21] P. Dimopoulos *et al.* [ETM Collaboration], arXiv:0810.2873 [hep-lat].
- [22] R. Frezzotti and G. C. Rossi, *JHEP* **0408** (2004) 007 [arXiv:hep-lat/0306014].
- [23] R. Baron *et al.* [ETM Collaboration], arXiv:0911.5061 [hep-lat].
- [24] D. Becirevic, P. Boucaud, J. P. Leroy, J. Micheli, O. Pene, J. Rodriguez-Quintero and C. Roiesnel, *Phys. Rev. D* **60** (1999) 094509 [arXiv:hep-ph/9903364].
- [25] F. de Soto and C. Roiesnel, *JHEP* **0709** (2007) 007 [arXiv:0705.3523 [hep-lat]].
- [26] M. Constantinou, V. Lubicz, H. Panagopoulos and F. Stylianou, *JHEP* **0910** (2009) 064 [arXiv:0907.0381 [hep-lat]].
- [27] S. Capitani, *Phys. Rept.* **382** (2003) 113 [arXiv:hep-lat/0211036].2005xn
- [28] M. Constantinou *et al.*, arXiv:1004.1115 [hep-lat].
- [29] J. A. Gracey, *Phys. Lett. B* **552** (2003) 101 [arXiv:hep-th/0211144].
- [30] P. Boucaud *et al.*, *Phys. Rev. D* **66** (2002) 034504 [arXiv:hep-ph/0203119].